FAILURE CONDITIONS OF A SATURATED REMOULDED CLAY

Thesis for the Degree of M. S.

MICHIGAN STATE UNIVERSITY

Abraham Kwan-Yuen Loh

1961

This is to certify that the

thesis entitled

"Failure Conditions of a Saturated
Remoulded Clay"

presented by

Abraham Kwan-Yuen Loh

has been accepted towards fulfillment
of the requirements for

M.S. degree in Civil Engineering

Major professor

Date Oct 11, 1961

O-169

ABSTRACT

FAILURE CONDITIONS OF A SATURATED
REMOULDED CLAY

by Abraham Kwan-Yuen Loh

An experimental study of the failure conditions under various states of applied stress has been made on a saturated remoulded clay. The purpose of the study was to examine the behavior of a clay under different stress states and the effect of stress changes on the shear strength.

In standard triaxial tests, the states of uniaxial or biaxial compression, superimposed on a hydrostatic stress state were examined. The effect of the intermediate principal stress on the yielding of clays was studied by using a hollow cylindrical sample, subjected to compression under various intermediate stress states. All tests were of the consolidated-undrained type. A Glacial Lake clay from Sault Ste. Marie, Michigan was used for the experiments.

It is shown that the Mohr effective stress failure envelopes are independent of the loading paths for each type of test, and that the intermediate principal stress has only a minor effect on the strength parameters of the clay. It is also shown that the stress-strain and pore-pressure change characteristics are dependent on the stress paths for each type of test.

Abraham Kwan-Yuen Loh

On the assumption that the material is isotropic and homogeneous, the test results have been used to compute a failure surface in the effective principal stress space. Results are compared with the generalized Coulomb's criterion. Good agreement is obtained, in spite of some minor deviations. Much experimental work remains to be carried out before the correctness of Coulomb's criterion can be established.

FAILURE CONDITIONS OF A SATURATED REMOULDED CLAY

By

ABRAHAM KWAN-YUEN LOH

A THESIS

Submitted to
Michigan State University
in partial fulfillment of the requirements
for the degree of

MASTER OF SCIENCE

Department of Civil Engineering

1961

ACKNOWLEDGEMENTS

The author is indebted to Dr. T. H. Wu, Department of Civil Engineering, without whose guidance and encouragement this thesis would not have been possible; he also wishes to express his sincere gratitude to Dr. L. E. Malvern, Department of Applied Mechanics, for his constructive comments and assistance, and to Dr. O. B. Andersland, Department of Civil Engineering, for his valuable suggestions. To his colleagues A. G. Douglas and R. D. Goughnour, the author wishes to express his sincere thanks for their criticism and assistance in the laboratory.

CONTENTS

LIST OF TABLES

LIST OF FIGURES

NOTATION

a	vertical intercept of a line drawn through top points of Mohr's circles
A_f	pore-pressure coefficient at failure
c	cohesion
$\bar{c}$	apparent cohesion in terms of effective stress
c_e	effective cohesion depending on the water content at failure only
C	arbitrary constant
D	deviator stress = $\sigma_{major} - \sigma_{minor}$
k	coordinate of apex of Coulomb's failure surface in principal stress space
K	ratio of external radius to internal radius (R_o/R_i)
M	proportionality factor
N_ϕ	flow coefficient = $\tan^2(45^o + \phi/2)$
$\bar{p}$	$\frac{1}{3}(\bar{\sigma}_1 + \bar{\sigma}_2 + \bar{\sigma}_3) \times \frac{1}{\sigma_c}$
p_i	internal pressure
p_o	external pressure
r	radius of element
R_c	radial distance on octahedral plane of principal stress space to failure surface in compression
R_e	radial distance on octahedral plane of principal stress space to failure surface in extension

R_i internal radius

R_o external radius

s shearing resistance

u pore-pressure

w water content

Δu pore-pressure change

ϵ axial strain

η angle between space diagonal and abscissa-axis in a stress-plane for axially-symmetrical stresses

ϕ angle of internal friction

$\bar{\phi}$ angle of shearing resistance in terms of effective stress

ϕ_e effective cohesion, depending on the water content at failure only

ψ slope angle of a line drawn through top points of Mohr's circles

σ normal compressive stress

$\bar{\sigma}$ effective normal compressive stress

σ_c consolidation pressure

σ_1, σ_2, σ_3 axial, circumferential and radial stresses respectively

$\bar{\sigma}_1$, $\bar{\sigma}_2$, $\bar{\sigma}_3$ effective, axial, circumferential and radial stresses respectively

σ'_1, σ'_2, σ'_3 principal stresses

σ''_1, σ''_2, σ''_3 stress space coordinates of projection onto an octahedral plane

τ shear stress

θ angle of inclination of shear plane

1. INTRODUCTION

The shear strength of clays is commonly defined by the Coulomb-Mohr failure criterion. The correctness of the Coulomb-Mohr criterion for a clay under various stress states has not been thoroughly investigated. It is, therefore, desirable to obtain experimental data on the failure conditions under various states of applied stress.

BISHOP and ELDIN (1953) and KIRKPATRICK (1957) found good agreement between values of the effective angles of shearing resistance of sand obtained from compression and extension tests, under drained conditions. KIRKPATRICK, in addition, studied the effect of the intermediate principal stress on the yielding of sands by using thick-walled cylindrical samples. He found that the values of the effective angle of shearing resistance so obtained were only slightly higher than those obtained from the conventional compression and extension tests. He also obtained an experimental failure surface in principal stress space which shows good agreement with the Coulomb-Mohr theory.

In contrast, HABIB (1953) and HAYTHORNTHWAITE (1960a) found that the values of the effective angle of shearing resistance of sand obtained in extension tests were considerably smaller than those obtained in compression tests, under drained conditions.

HAYTHORNTHWAITE (1960b) also studied the yield conditions of a remoulded silt by subjecting hollow cylindrical samples to combined torsion and compression, under drained conditions. He obtained an experimental failure surface in principal stress space which shows substantial departure from the Coulomb-Mohr theory.

HENKEL (1959, 1960) and PARRY (1960) reported good agreement between values of the effective angle of shearing resistance obtained from compression and extension tests on normally-consolidated remoulded clays, under both drained and undrained conditions. Experimental information on the condition of failure for clays under intermediate stress states is not available.

In view of the conflicting evidence presented by the aforementioned investigators and the need for experimental data on the condition of failure for clays under various intermediate stress states, a series of consolidated-undrained triaxial tests has been carried out on a saturated remoulded clay. The general objectives were: to examine the behavior of clays under different stress states; to study the effect of the intermediate principal stress on the shear strength of clays; and to obtain an experimental failure surface in principal stress space, in order that the experimental evidence can be compared with the Coulomb-Mohr predictions.

2. THEORETICAL CONSIDERATIONS

2.1. Shearing Resistance of a Cohesive Soil

The shearing resistance of a cohesive soil, in general, has been defined by Coulomb as follows:

$$s = c + \sigma \tan \phi \tag{1}$$

where
- s is the shearing resistance
- c is the cohesion
- σ is the normal compressive stress
- ϕ is the angle of internal friction

The parameters c and ϕ in the preceding equation are assumed to be constant and are independent of the state of stress preceding failure. The rational use of Coulomb's Law requires an understanding of the many complex factors affecting the shear strength of clays. It is of utmost importance to realize that c and ϕ are not constant soil properties but are merely empirical coefficients, which may vary for a given soil depending on a number of variables (stress history, drainage conditions, water content or void ratio, structure, speed of shear and others). In the conventional triaxial test, the values of c and ϕ obtained depend on the stress history of the soil as well as the applied stress conditions.

Terzaghi (1936) concluded that the stress conditions for failure in soils as well as the volume changes, depend solely on the intensity of effective stresses. The stress conditions for failure in soils therefore depend exclusively on the effective stress which is given by

$$\bar{\sigma} = \sigma - u \tag{2}$$

where σ is the total stress

$\bar{\sigma}$ is the effective stress

and u is the pore-pressure.

In terms of effective stresses, Coulomb's failure criterion for the shearing resistance of a saturated clay may be expressed by the following:

$$s = \bar{c} + \bar{\sigma} \tan \bar{\phi} \tag{3}$$

where s denotes the shearing resistance

$\bar{c}$ denotes the apparent cohesion

$\bar{\sigma}$ denotes the effective normal stress on the failure plane considered

and $\bar{\phi}$ denotes the angle of shearing resistance.

Hvorslev (1937, 1960) expressed the shear strength of a cohesive soil in terms of the fundamental soil properties as follows:

$$s = c_e + \bar{\sigma} \tan \phi_e \tag{4}$$

where s is the shearing resistance

c_e is the effective cohesion, depending on the water content at failure only.

$\bar{\sigma}$ is the effective normal stress on the failure plane

and ϕ_e is the effective angle of friction.

The effective angle of friction ϕ_e is a property of the material, whereas the angle of shearing resistance $\bar{\phi}$ is merely the rate of increase of overall shear strength with pressure. In the case of a saturated normally-consolidated clay, for instance, the shear strength, in terms of effective stresses, may be expressed as follows:

$$s = \bar{\sigma} \tan \bar{\phi}$$

The apparent cohesion $\bar{c}$ is equal to zero. The term $\bar{\sigma} \tan \bar{\phi}$ includes both the effective cohesion and the effective friction and may be expressed in terms of Hvorslev's parameters as follows:

$$\bar{\sigma} \tan \bar{\phi} = c_e + \bar{\sigma} \tan \phi_e .$$

2. 2. <u>Mohr's Theory of Rupture</u>

The state of stress at a point may be represented graphically by a plot known as the Mohr diagram. This diagram is of the utmost value in the study of stress conditions. Mohr's rupture theory may be expressed by the statement that there exists for a material a boundary called Mohr Envelope such that a Mohr circle within the envelope represents a stable condition, whereas a circle tangent to the envelope represents failure on the plane denoted by the point of tangency. The Mohr envelope or line of rupture is a property of the material, whereas the Mohr circle depends only on the stresses caused by the loading, and it is independent of what the material may be.

The hypothesis formulated by Mohr, demonstrated in Fig. 1 can be summarized as follows:

1. The line of rupture is independent of the means by which it is obtained.
2. The line of rupture is independent of the intermediate principal stress.
3. The angle between the line of rupture and a vertical is equal to the angle between planes of rupture in the material at failure.

Mohr's representation of the stress condition for failure is extremely useful in solving problems in soil mechanics in that Coulomb's criterion can be readily expressed by means of the Mohr's diagram. In Fig. 2 is shown Mohr's graphical representation of the principal stress components acting on a soil element. Assuming that the Mohr failure envelope is the straight line $s = c + \sigma \tan \phi$, the geometrical relationship in Mohr's diagram yields equations (5), (6), (7) and (8) in the following paragraph.

The Mohr's diagram shown in Fig. 2 shows that the normal and shear stresses on any plane can be expressed as

$$\sigma = \sigma_1 \cos^2\theta + \sigma_3 \sin^2\theta = \frac{\sigma_1 + \sigma_3}{2} + \frac{1}{2}(\sigma_1 - \sigma_3) \cos 2\theta \qquad (5)$$

$$\tau = (\sigma_1 - \sigma_3) \sin\theta \cos\theta = \frac{\sigma_1 - \sigma_3}{2} \sin 2\theta \qquad (6)$$

Mohr's envelope for Coulomb's failure criterion is

$$s = c + \sigma \tan \phi.$$

Hence,

$$\sigma_1 - \sigma_3 = 2c \cos \phi + (\sigma_1 + \sigma_3) \sin \phi \tag{7}$$

which can be written as

$$\begin{aligned} \sigma_1 &= \sigma_3 \tan^2 (45^\circ + \phi/2) + 2c \tan (45^\circ + \phi/2) \\ &= \sigma_3 N_\phi + 2c\sqrt{N_\phi} \end{aligned} \tag{8}$$

where $\quad N_\phi = \tan^2 (45^\circ + \phi/2).$

2. 3. Yield Surface in Principal Stress Space

Coulomb's failure criterion can be generalized to extend its validity to three-dimensional representation of stress conditions in stress fields (Drucker, 1953; Shield, 1955). This interpretation of Coulomb's criterion leads to a yield surface for three-dimensional stress fields (Hill, 1950).

In principal stress space, the yield surface is a right hexagonal pyramid equally inclined to the $\sigma'_1, \sigma'_2, \sigma'_3$ axes, with its apex on the line $\sigma'_1 = \sigma'_2 = \sigma'_3$. The hexagon is irregular since the yield stress in tension differs from that in compression (Shield, 1955). The yield surface in principal stress space is shown in Fig. 3, bounded by 6 planes, the equations of which are as follows:

$$\left.\begin{aligned}
\sigma'_1 &= \sigma'_3 N_\phi + 2c\sqrt{N_\phi} \\
\sigma'_3 &= \sigma'_1 N_\phi + 2c\sqrt{N_\phi} \\
\sigma'_2 &= \sigma'_1 N_\phi + 2c\sqrt{N_\phi} \\
\sigma'_1 &= \sigma'_2 N_\phi + 2c\sqrt{N_\phi} \\
\sigma'_3 &= \sigma'_2 N_\phi + 2c\sqrt{N_\phi} \\
\sigma'_2 &= \sigma'_3 N_\phi + 2c\sqrt{N_\phi}
\end{aligned}\right\} \tag{9}$$

where as before $\qquad N_\phi = \tan^2 (45^\circ + \phi/2)$

The apex of the yield surface is determined by the equation

$$\sigma'_1 = \sigma'_2 = \sigma'_3 = k$$

where

$$k = \frac{2c\sqrt{N_\phi}}{1-N_\phi} = -c \cot \phi \tag{10}$$

Fig. 4A shows the right section of the yield surface by the octahedral plane $\sigma'_1 + \sigma'_2 + \sigma'_3 = 0$. Right sections by other planes $\sigma'_1 + \sigma'_2 + \sigma'_3 =$ constant are similar in shape but are of varying size, depending on the distance along the space diagonal at which they are taken. It is shown in the following paragraphs that the ratio $R_c = OC : R_e = OE$ in Fig. 4A is independent of c, when this parameter c is a constant.

Fig. 4B shows the stress system and the stress-plane that can be investigated in the standard triaxial test. Fig. 4C shows the Mohr effective stress failure envelopes and the effective stress-plane for axially-symmetrical stresses. The right section of the yield surface by the octahedral plane FBADG, whose equation is $\bar{\sigma}_1 + \bar{\sigma}_2 + \bar{\sigma}_3 = \sigma_a$ is similar in shape to the one shown in Fig. 4A. The space diagonal in Fig. 4C defines the isotropic stress condition where $\bar{\sigma}_1 = \bar{\sigma}_2 = \bar{\sigma}_3$. If the all-round stress at point A is σ_a the stresses at points B (compression) and D (extension) can be obtained as follows:

At point B (compression), $R_c = AB$,

$$\bar{\sigma}_1 = \sigma_a + R_c \cos \eta = \sigma_a + R_c \sqrt{2/3}$$

$$\bar{\sigma}_3 = \sigma_a - \sqrt{1/2}\, R_c \sin \eta = \sigma_a - R_c \sqrt{1/6}$$

and

$$R_c = (\bar{\sigma}_1 - \bar{\sigma}_3) \sqrt{2/3}.$$

At point D (extension), $R_e = AD$,

$$\bar{\sigma}_1 = \sigma_a - R_e \cos \eta = \sigma_a - R_e \sqrt{2/3}$$

$$\bar{\sigma}_3 = \sigma_a + \sqrt{1/2}\, R_e \sin \eta = \sigma_a + R_e \sqrt{1/6}$$

and

$$R_e = (\bar{\sigma}_3 - \bar{\sigma}_1) \sqrt{2/3}.$$

On the right section by the plane $\bar{\sigma}_1 + \bar{\sigma}_2 + \bar{\sigma}_3 = 0$ through the origin O (Fig. 4C), $\sigma_a = 0$. We have then in a compression test

$$\bar{\sigma}_1 = R_c \sqrt{2/3}, \qquad \bar{\sigma}_3 = -R_c \sqrt{1/6}, \qquad R_c = (\bar{\sigma}_1 - \bar{\sigma}_3) \sqrt{2/3}$$

and in an extension test

$$\bar{\sigma}_1 = -R_e \sqrt{2/3}, \qquad \bar{\sigma}_3 = +R_e \sqrt{1/6}, \qquad R_e = (\bar{\sigma}_3 - \bar{\sigma}_1)\sqrt{2/3}$$

where $\bar{\sigma}_1, \bar{\sigma}_3$ are the effective stress components

R_c is the radial distance in compression on the plane $\bar{\sigma}_1 + \bar{\sigma}_2 + \bar{\sigma}_3 = 0$

and R_e is the radial distance in extension on the plane $\bar{\sigma}_1 + \bar{\sigma}_2 + \bar{\sigma}_3 = 0$.

Using equation (7), we obtain

$$R_c = \frac{2c \cos\phi \sqrt{6}}{3 - \sin\phi} \tag{11}$$

$$R_e = \frac{2c \cos\phi \sqrt{6}}{3 + \sin\phi} \tag{12}$$

On dividing, we have

$$\frac{R_c}{R_e} = \frac{3 + \sin\phi}{3 - \sin\phi} \tag{13}$$

It is to be noted that this ratio R_c/R_e is independent of c, when c is a constant.

It can be seen from equation (13) or from equation (7) that when $\phi = 0$, Coulomb's criterion becomes Tresca's yield condition (maximum shear stress at yield equal to a constant, Hill, 1950) where $R_c/R_e = 1$. The corresponding right section by the plane $\sigma'_1 + \sigma'_2 + \sigma'_3 = 0$ is then a regular hexagon with the yield stress in tension equal to that in compression.

To study the validity of Coulomb's criterion in three-dimensional stress fields, the experimental stress points at failure can be projected onto a chosen octahedral plane. These points may then be compared with Coulomb's failure surface. The projection of any stress point at failure on this octahedral plane is equal to the point where the straight line joining the stress point and the apex $\sigma'_1 = \sigma'_2 = \sigma'_3 = k$ of Coulomb's yield surface intersects the octahedral plane. Any straight line joining a stress point in stress space and the apex of Coulomb's yield surface can be expressed by the following:

$$\frac{\sigma_1 - \sigma''_1}{\sigma_1 - k} = \frac{\sigma_2 - \sigma''_2}{\sigma_2 - k} = \frac{\sigma_3 - \sigma''_3}{\sigma_3 - k} \tag{14}$$

where σ_1, σ_2, σ_3 are the experimental failure stresses and σ''_1, σ''_2, σ''_3 are the stress space coordinates of the projection of the experimental point onto the plane

$$\sigma''_1 + \sigma''_2 + \sigma''_3 = C \tag{15}$$

From (14) we have

$$-\sigma''_1(\sigma_2 - k) + \sigma''_2(\sigma_1 - k) + k(\sigma_2 - \sigma_1) = 0 \tag{16}$$

$$-\sigma''_1(\sigma_3 - k) + \sigma''_3(\sigma_1 - k) + k(\sigma_3 - \sigma_1) = 0 \tag{17}$$

By solving simultaneously (15), (16) and (17) we obtain

$$\sigma''_1 = \frac{-k(2\sigma_1 - \sigma_2 - \sigma_3) + C(\sigma_1 - k)}{\sigma_1 + \sigma_2 + \sigma_3 - 3k} \tag{18}$$

Similarly, we also obtain

$$\sigma''_2 = \frac{-k(2\sigma_2 - \sigma_3 - \sigma_1) + C(\sigma_2 - k)}{\sigma_1 + \sigma_2 + \sigma_3 - 3k} \tag{18}$$

$$\sigma''_3 = \frac{-k(2\sigma_3 - \sigma_1 - \sigma_2) + C(\sigma_3 - k)}{\sigma_1 + \sigma_2 + \sigma_3 - 3k} \tag{18}$$

In the case of a normally-consolidated clay, in terms of effective stresses, $c = 0$ and the apex of Coulomb's yield surface is at the origin. For points on the Coulomb's surface, we have then from (9) and (18)

in a compression test

$$\left.\begin{aligned} \sigma''_1 &= \frac{C\,N_\phi}{N_\phi + 2} \\ \sigma''_2 = \sigma''_3 &= \frac{C}{N_\phi + 2} \end{aligned}\right\} \tag{19}$$

and in an extension test

$$\left.\begin{aligned} \sigma''_1 &= \frac{C}{2N_\phi + 1} \\ \sigma''_2 = \sigma''_3 &= \frac{CN_\phi}{2N_\phi + 1} \end{aligned}\right\} \tag{20}$$

for a normally-consolidated clay.

Equations (19) and (20) yield

$$R_c = (\sigma''_1 - \sigma''_3) \cdot M = \frac{C\,(N_\phi - 1)}{N_\phi + 2} \cdot M$$

$$R_e = (\sigma''_3 - \sigma''_1) \cdot M = \frac{C\,(N_\phi - 1)}{2\,N_\phi + 1} \cdot M$$

for a normally-consolidated clay, where M is a proportionality factor.

On dividing, we have as before (13)

$$\frac{R_c}{R_e} = \frac{3 + \sin\phi}{3 - \sin\phi}$$

3. EXPERIMENTAL PROGRAM

3.1. Materials Used

The clay used in the testing program was obtained from Sault Ste. Marie, Michigan. Details of the geotechnical properties of the Glacial Lake clay in its natural state have been published (Wu, 1958). The index properties are given in Table 1 below.

Table 1. Index properties of Michigan clay

L. L. %	P. L. %	P. I. %	Clay fraction %	Activity
55	23	32	60	0.53

3.2. Sample Preparation

Bulk samples of air-dried clay were thoroughly remoulded and mixed with distilled water to a consistency corresponding to a water content of 40-45%. Hollow cylindrical samples were prepared by injecting the remoulded clay into a mould provided by the formers, described in Chapter 4 "Apparatus," by means of a jack. Cylindrical samples for the standard triaxial cell were prepared by the conventional procedure described by Bishop and Henkel (1957).

The remoulded clay samples were normally-consolidated under all-round pressures of 3 or 4 kg./cm.^{2} before the shear tests were carried out. Filter paper side drains were used to accelerate the consolidation process. Volume changes were measured throughout the consolidation process. Water contents were measured before consolidation and after completion of the shear tests.

3.3. The Shear Tests

Consolidated-undrained triaxial tests were performed on the remoulded clay. Descriptions of the stress changes applied to the samples are given below, together with the abbreviations used to describe the tests:

UC1	$\sigma_1 > \sigma_2 = \sigma_3$ = constant.	Axial stress increased, radial stress constant.
UC2	$\sigma_1 > \sigma_2 = \sigma_3$, σ_1 = constant.	Axial stress constant, radial stress decreased.
UI1	$\sigma_2 > \sigma_1 > \sigma_3$	Axial stress increased first, followed by increasing all three, the axial, radial and circumferential stresses.
UI2	$\sigma_1 > \sigma_2 > \sigma_3$, σ_2, σ_3 = constant.	All stresses increased first; radial and circumferential stresses then maintained constant, followed by axial stress increase.
UI3	$\sigma_2 > \sigma_1 > \sigma_3$, σ_1 = constant.	Axial stress increased first; and then maintained constant, followed by increasing radial and circumferential stresses.
UE1	$\sigma_1 < \sigma_2 = \sigma_3$ = constant.	Axial stress decreased, radial stress constant.
UE2	$\sigma_1 < \sigma_2 = \sigma_3$, σ_1 constant.	Radial stress increased, axial stress constant.

$\sigma_1, \sigma_2, \sigma_3$ represent the axial, circumferential and radial stresses respectively.

UE1, UE2 and UC2 tests were carried our on the standard triaxial cell, whereas UC1, UI1, UI2 and UI3 tests were carried out on the hollow-cylinder triaxial cell.

Pore-pressures were measured in all the tests. UC1, UI1, UI2 and UI3 tests were carried out with controlled stress increments, allowing 10 minutes for equilibrium to be attained for each increment. Usually, thirty to thirty-five increments were required to reach failure UC2, UE1 and UE2 tests were carried out at controlled rate of strain of 2-3% per hour. The specimens usually reached failure in about 5 hours after the initial loading.

Area corrections have been applied in the evaluation of all test data (Bishop and Henkel, 1957). Corrections for membrane and filter strip restraint have not been applied to the results. All tests were run against a back pressure of 1 to 1.5 kg./cm.^{2}, maintained for at least 10 hours before testing, in order to eliminate the possibility of developing negative pore-pressures, and to force into solution any free or entrapped air, which may exist in the sample or in the testing apparatus.

In the evaluation of the test results, the elastic theory of thick-walled cylinders has been used. According to this theory (Timoshenko, 1940), plane sections perpendicular to the longitudinal axis are assumed to remain plane and consequently the longitudinal strain is independent of the radius. It can be shown that for a thick-walled cylinder subjected to internal and external pressures, the radial and circumferential stresses can be expressed as follows:

$$\sigma_2 = \frac{p_i - K^2 p_o}{K^2 - 1} + \frac{(p_i - p_o)}{r^2} \cdot \frac{R_o^{\,2}}{K^2 - 1} \tag{21}$$

$$\sigma_3 = \frac{p_i - K^2 p_o}{K^2 - 1} - \frac{(p_i - p_o)}{r^2} \cdot \frac{R_o^{\,2}}{K^2 - 1} \tag{22}$$

where σ_2 is the normal circumferential stress

σ_3 is the normal radial stress

r is the radius of the elment

R_i is the internal radius

R_o is the external radius

p_i is the internal pressure

p_o is the external pressure

$K = R_o/R_i$.

and the conventional positive sign convention for tension is adopted.

From (21) and (22), we have

at $r = R_o$

$$\left.\begin{aligned} \sigma_2 &= \frac{2\,p_i - p_o(K^2 + 1)}{K^2 - 1} \\ \sigma_3 &= -p_o \end{aligned}\right\} \tag{23}$$

and at $r = R_i$

$$\left.\begin{aligned} \sigma_2 &= \frac{p_i(K^2 + 1) - 2K^2 p_o}{K^2 - 1} \\ \sigma_3 &= -p_i \end{aligned}\right\} \tag{24}$$

Assuming a linear stress distribution across the cylinder wall for both σ_2 and σ_3, from (23) and (24), the average circumferential and radial stresses can be expressed as follows:

$$\left.\begin{aligned} \sigma_{2\,av} &= -[p_i + \frac{3K^2 + 1}{2(K^2 - 1)}(p_o - p_i)] \\ \sigma_{3\,av} &= -(p_i + p_o)/2 \end{aligned}\right\} \tag{25}$$

Equation (25) was used to calculate the stresses.

4. APPARATUS

UEl, UE2 and UC2 tests were carried out on the standard triaxial cell, whereas UCl, UIl, UI2 and UI3 tests were carried out on the hollow cylinder triaxial cell described below. Details of the hollow cylinder triaxial cell are shown in Fig. 5.

The construction of the apparatus was mainly governed by the necessity to have a complete pressure seal between the bore and the outside chamber. An air release valve at Y and rubber O-rings at P in the sample end-piece F and at Q in the base adaptor S have been provided for this purpose.

The principal features to be noted are:

The Removable Top Cap and Pressure Cylinder

A transparent plexiglass cylinder M, fitted between rubber gaskets and held against the top cap C and the base J by 4 steel tie bars, is used. The top cap is provided with an oil filler valve at B and an air release valve at D.

The Loading Ram

A 1/2" diameter stainless steel ram is used. It is fitted inside the bronze bushing in the top cap C in order to minimize friction and leakage.

The Base and the Base Adaptor

The base J is provided with connections for the outside chamber fluid pressure at L, the bore chamber fluid pressure at K, and for pore-pressure measurements at W and drainage at H in the Pedestal X.

The base adaptor S was made removable to allow for the seal of the inner membrane at Q. It is held tight against the pedestal X by a tightening bolt and nut at R, provided with a rubber O-ring at T.

The Sealing Cap and the Sample End-piece

Seal between the bore and the outside of the sample G is provided by the air release valve Y in the sealing cap O and the rubber O-ring at P in the sample end-piece F. The sealing cap O is screwed onto the threaded sample end-piece F and the outside membrane is sealed off by O-rings at U and V.

Rubber Membranes

The sample G is enclosed between two rubber membranes, forming a hollow cylinder of 3 inches in inside diameter, 4 inches in outside diameter snd 5 inches in height. The membranes are 0. 013" thick, supplied by Testlab Corporation in Chicago, Illinois.

The outside and the bore chamber pressures are each controlled by a Norwegian Constant Pressure Cell (Andresen and Simons, 1960). The pressure difference between the outside and the bore chambers is measured by a mercury manometer. Pore-pressures are measured by connecting the sample to a manometer and a Bourdon pressure gauge, through a Null Indicator (Andresen and Simons, 1960).

The Formers for Preparing Hollow Cylindrical Specimens

Hollow cylindrical specimens were prepared by using a mould formed by an inner plexiglass former and an outer split aluminum jacket shown in Fig. 6. The remoulded clay was placed in a 6" hollow steel cylinder and injected into the mould, by means of a jack connected to the steel cylinder. The sample end-piece was then placed on the sample after the trimming of the top of the sample had been carried out. The inside membrane was secured to the sample end-piece by a rubber band. The inner former was then withdrawn and the sealing cap was screwed tight onto the threaded sample end-piece. The outer former was removed and the sample was ready for testing after placing O-rings on the outside membrane at U and V (Fig. 5).

The clay specimen, prepared in this way, is likely to be slightly over-consolidated due to the injecting pressure, but it is believed that the magnitude of the over-consolidation pressure would be of insignificant importance. It was found that if the consistency of the clay was such that its water content was below about 40%, difficulties were encountered during the injection process.

5. RESULTS

Applied stresses and pore-pressures were recorded for each test against axial strain. Complete details of each test are shown in Figs. 7-13 and in Tables 11-17 in Appendix 2, "Data," together with sample calculations for each type of test. In this paper failure is defined as the peak point on the deviator stress-strain curve.

5.1. Deviator Stress

Values of maximum deviator stress (designated as D) are shown plotted against axial strain in Figs. 7-13. For comparison, typical test results from each type of test have been plotted on the same diagram in Fig. 14.

In all cases, with the exception of the UE1 and UE2 tests, the deviator stress increases rapidly with strain in the beginning of the test, and remains virtually constant at failure. In the case of the UE1 and UE2 tests, similar behavior of the deviator stress is observed, except that the deviator stress decreases after a maximum has been reached.

The average maximum deviator stress, expressed in terms of the consolidation pressure σ_c, for each type of test is summarized in Table 2 below.

Table 2. Deviator stress at failure

Test	D_f/σ_c	$D_f/D_{f'}$ UC1
UC1	0.82	1.00
UC2	0.72	0.88
UI1	0.91	1.11
UI2	0.83	1.01
UI3	0.99	1.21
UE1	0.62	0.76
UE2	0.52	0.64

It is interesting to note that the so-called "undrained shear strength" $D_f/2$ varies with the type of test and appears to be dependent upon the loading path. It can be seen that the difference in undrained shear strength, expressed in terms of the consolidation pressure, obtained from the various types of tests, is quite remarkable. The only close agreement is cited between the UC1 and UI2 tests. The differences can only be explained by the fact that the pore-pressure behaves differently in each type of test. It appears that a Tresca-type condition, D = constant, cannot be used as a failure criterion.

5.2. Pore-pressure

Values of pore-pressure change (designated as Δu) are shown plotted against axial strain in Figs. 7-13. For comparison, typical test results from each type of test have been plotted on the same diagram in Figs. 15A and 15B.

The UC1, UI1 and UI2 tests show an initial rapid rate of pore-pressure increase, reducing to a negligible rate of change at failure. The UC2 test shows a small initial rapid increase, followed by a rapid decrease in pore-pressure. The rate of decrease then becomes negligible during the remainder of the test. The decrease continues after failure has been reached. The UE1 and UE2 tests show a small initial rapid pore-pressure decrease, followed by an increase in pore-pressure which is considerably less than that for the UC1, UI1 and UI2 tests at failure. The rate of pore-pressure change at failure is again negligible. The UI3 test shows an initial rapid rate of pore-pressure increase, reducing to a negligible rate of change at failure.

The average pore-pressure at failure, expressed in terms of the consolidation pressure σ_c, and the pore-pressure parameter A_f (Skempton, 1954) for each type of test is summarized in Table 3 below.

It can be seen from Table 3 that A_f is dependent on the stress path for each type of test and varies with the type of test.

Table 3. Pore-pressure at failure

Test	$\frac{(\Delta u)_f}{\sigma_c}$	$A_f = \frac{(\Delta u)_f}{D_f}$
UC1	+0.64	+0.78
UC2	-0.33	-0.46
UI1	+0.63	+0.69
UI2	+0.63	+0.76
UI3	+0.40	+0.41
UE1	+0.08	+0.13
UE2	+0.77	+1.48

5.3. Effective Principal Stresses

Values of the effective principal stresses (designated as $\bar{\sigma}_1, \bar{\sigma}_2, \bar{\sigma}_3$) are shown plotted against axial strain in Figs. 7-13.

In the UC1 and UC2 tests, the axial stress is the major principal stress while both the intermediate and minor principal stresses are equal to the radial stress. In the UE1 and UE2 tests, however, the axial stress becomes the minor principal stress while both the major and intermediate principal stresses are now equal to the radial stress.

In all the remaining tests, where the intermediate principal stress is different from the major and the minor principal stresses the radial stress $\bar{\sigma}_3$ is always the minor principal stress. Whether the axial or circumferential stress is the major or the intermediate principal stress depends on the method of applying the stresses. In the UI1 and UI3 tests, a change of the circumferential stress $\bar{\sigma}_2$ from the intermediate to the major principal stress takes place during the test. In the UI2 test, however, a change of the circumferential stress $\bar{\sigma}_2$ from the major to the intermediate principal stress takes place during the test.

In all cases, all the three principal stresses remain virtually constant at failure.

The average effective principal stresses at failure, expressed in terms of the consolidation pressure σ_c and the effective principal stress ratio are summarized in Table 4 below.

Table 4. Effective principal stresses at failure

Test	$\bar{\sigma}_1/\sigma_c$	$\bar{\sigma}_2/\sigma_c$	$\bar{\sigma}_3/\sigma_c$	$(\bar{\sigma}$ major + $\bar{\sigma}$ minor$)$	$\frac{\bar{\sigma}\text{ major}}{\bar{\sigma}\text{ minor}}$
UC1	1.16	0.34	0.34	1.49	3.47
UC2	1.12	0.36	0.36	1.49	3.11
UI1	1.12	1.31	0.40	1.71	3.32
UI2	1.15	0.61	0.33	1.48	3.54
UI3	0.88	1.43	0.44	1.87	3.25
UE1	0.26	0.88	0.88	1.14	3.39
UE2	0.43	0.94	0.94	1.37	2.18

It is interesting to note from Table 4, that with the exception of the UE2 test, the effective principal stress ratio at failure changes very little with the type of test. For a normally-consolidated clay, Coulomb's criterion, in terms of effective stresses, can be expressed as

$$\bar{\sigma}_i = \bar{\sigma}_j N_\phi$$

where as before

$$N_\phi = \tan^2 (45^\circ + \bar{\phi}/2)$$

and $\bar{\sigma}_i$, $\bar{\sigma}_j$ denote the effective major and minor principal stresses respectively. The fact that $\bar{\sigma}_i/\bar{\sigma}_j$ = constant as shown implies that Coulomb's criterion is valid for clays under various intermediate stress states.

5. 4. Axial Strain at Failure

Although the axial strain at failure cannot be defined with great accuracy, it appears that within experimental error, the axial strain at failure varies with the stress path for each type of test. The average axial strain at failure for each type of test is summarized in Table 5 below.

Table 5. Axial strain at failure

Test		Axial strain at failure %
UC1	$\sigma_1 > \sigma_2 = \sigma_3$ = constant	13. 4
UC2	$\sigma_1 > \sigma_2 = \sigma_3$, σ_1 = constant	14. 6
UI1	$\sigma_2 > \sigma_1 > \sigma_3$	2. 7
UI2	$\sigma_1 > \sigma_2 > \sigma_3$, σ_2, σ_3 = constant	7. 4
UI3	$\sigma_2 > \sigma_1 > \sigma_3$, σ_1 = constant	1. 3
UE1	$\sigma_1 < \sigma_2 = \sigma_3$ = constant	10. 7
UE2	$\sigma_1 < \sigma_2 = \sigma_3$, σ_1 = constant	7. 0

The interesting feature to be noted is the wide range of axial strains at failure, varying from 1. 3% to 14. 6%. The wide range of variation of axial strains is to be expected since the axial strains are not the major principal strains in some of the tests. In the UCI, UC2 and U12 tests where the axial stress σ_1 is the major principal stress at failure, a variation of 7. 4% to 14. 6% is noted. Although a comparison of axial strains would be inconsistent for the other tests where the axial stress σ_1 is not the major principal stress at failure, variation between UIl and U13 tests, UEl and UE2 tests is also observed. The results obtained appear to be in agreement with the formulations by Levy-Mises (Hill, 1950) that the principal axes of stress and strain coincide.

5. 5 Failure Conditions

Details pertinent to the condition at failure for each type of test have been summarized and are shown in Table 6. The subscript f has been used to designate the principal stresses, pore-pressures, maximum deviator stress, axial strain or water content at failure. The mode of failure, observed from visual inspection of the specimen after failure, of each type of test has been described and is also given in Table 6.

Table 7 summarizes the stress conditions at failure for the various types of tests. For ease of comparison the stresses at failure have been expressed in terms of the consolidation pressure.

The test results for the stress conditions at failure obtained for Michigan clay in this investigation have been compared with those obtained on Weald clay by Parry (1960) and are presented in Table 8. Although the nature of Michigan clay is expected to be different from Weald clay, it is interesting to note that the trend is remarkably similar. It is to be noted that for both clays, the undrained shear strength $D_f/2$ and the pore-pressure change characteristics are dependent on the stress paths for each type of test and vary with the type of test, and that, for all practical purposes, the effective principal stress ratio at failure is independent of the stress path, irrespective of the type of test.

5.6. Mohr Failure Envelopes

The Mohr effective stress failure envelopes and the corresponding loading paths for different types of tests are shown in Figs. 16A and 16B. Instead of plotting the Mohr failure circles, the top point of each failure circle has been plotted. If a and ψ are the vertical intercept and the slope angle for the straight line through such points, it can be shown that

$$\sin \bar{\phi} = \tan \psi, \qquad \text{and } \bar{c} = a/\cos \bar{\phi}.$$

Fig. 17A shows the Mohr effective stress failure envelope obtained from UC1, UC2 and UE1 tests. Fig. 17B shows the Mohr effective stress failure envelope obtained from UI1, UI2 and UI3 tests.

It can be seen that the values of $\bar{\phi}$ from the different types of tests do not differ by more than 1^{o}. A value of 33^{o} is obtained from UI1, UI2 and UI3 tests where the intermediate principal stress is different from the major and the minor principal stresses, whereas a value of 32^{o} is obtained from UC1, UC2 and UE1 tests where the intermediate principal stress is equal to either the major or the minor principal stresses. In a stress system where the intermediate principal stress is different from the major and the minor principal stresses, the Coulomb-Mohr theory underestimates the shear strength of a clay. The error, however, is slight and has very little practical significance.

The effective strength parameters obtained from the different types of tests are summarized in Table 9.

5.7. Yield Surface

Fig. 18 shows the experimental stress points representing failure projected onto the plane $\sigma''_1 + \sigma''_2 + \sigma''_3 = 1$. Coulomb's criterion, based on the effective strength parameters of $\bar{c} = 0$ and $\bar{\phi} = 32^{o}$ obtained from compression and extension tests on the standard triaxial cell, is shown as dotted lines in the same figure.

The representation of experimental stress points projected onto the plane $\sigma''_1 + \sigma''_2 + \sigma''_3 = 1$ is readily obtained by using equation (18) as follows:

For $\bar{c} = 0$, $k = 0$ and with $C = 1$ equation (18) becomes

$$\sigma''_1 = \frac{\sigma_1}{\sigma_1 + \sigma_2 + \sigma_3}, \qquad \sigma''_2 = \frac{\sigma_2}{\sigma_1 + \sigma_2 + \sigma_3}, \qquad \sigma''_3 = \frac{\sigma_3}{\sigma_1 + \sigma_2 + \sigma_3}$$

The projected effective principal stress space coordinates of the experimental stress points from each type of test are shown in Table 10.

The representation of Coulomb's criterion projected onto the plane $\sigma''_1 + \sigma''_2 + \sigma''_3 = 1$ is readily obtained by using equation (19) and (20) as follows:

$$\text{for } \bar{c} = 0 \text{ and } \bar{\phi} = 32^{o} \qquad N_{\phi} = 3.25.$$

With $C = 1$, we have in a compression test

$$\sigma''_1 = \frac{C\,N_{\phi}}{N_{\phi} + 2} = \frac{3.25}{2 + 3.25} = 0.62.$$

$$\sigma''_2 = \sigma''_3 = \frac{C}{N_{\phi} + 2} = \frac{1}{3.25 + 2} = 0.191$$

and in an extension test

$$\sigma''_1 = \frac{C}{2N_{\phi} + 1} = \frac{1}{2 \times 3.25 + 1} = 0.134$$

$$\sigma''_2 = \sigma''_3 = \frac{C\,N_{\phi}}{2N_{\phi} + 1} = \frac{3.25}{2 \times 3.25 + 1} = 0.434$$

It can be seen that the experimental data are in good agreement with Coulomb's prediction. The test data also show minor departure from Coulomb's criterion. Since only a limited number of triaxial tests have been carried out in the present investigation, a considerably greater volume of experimental evidence is needed before any strong assertions can be made.

6. CONCLUSIONS

The conclusions summarized below reflect the findings of this investigation and are limited to the soil used, the methods of sample preparation and the testing procedure employed:

1. The undrained shear strength of a clay is dependent on the loading path for each type of test and varies with the type of test. The variation may be explained by the different pore-pressure behavior under different applied stress changes.

2. The pore-pressure change characteristics are dependent on the loading path for each type of test and vary with the type of test.

3. The effective principal stress ratio at failure, for all practical purposes, is independent of the loading path, irrespective of the type of test.

4. The axial strain at failure appears to vary with the loading path for each type of test. Test results appear to be in agreement with the concept that the principal axes of stress and strain are coincident.

5. The Mohr effective stress failure envelopes are independent of the loading paths for each type of test. In a stress system where the intermediate principal stress is different from the major and the minor principal stresses, the Coulomb-Mohr theory underestimates the shear strength of a clay.

6. The validity of Coulomb's criterion in three-dimensional stress fields has been studied. Test results show that the experimental failure surface is, in general, in good agreement with Coulomb's prediction, although minor deviations are noted.

7. In this investigation, it has been tacitly assumed that the elastic theory is valid in the calculation of stresses at failure. The fact that the behavior of clays is not truly elastic has not been considered. In the evaluation of the stresses and strains at failure, an error or inaccuracy is likely to be introduced by assuming that the material is fully elastic. It is believed that the elasto-plastic and/or the plastic solution would be more satisfactory in the understanding of the behavior of clays.

8. So far it has not been possible to relate the stresses with the strains measured in the various types of tests. For a complete understanding of the deformation behavior of clays, it appears necessary that stress and strain should be related. In the future, it is hoped to extend the range of tests to include stress states such as torsion, combined torsion and compression, in order that some of the limitations on the validity of the test data can be eliminated.

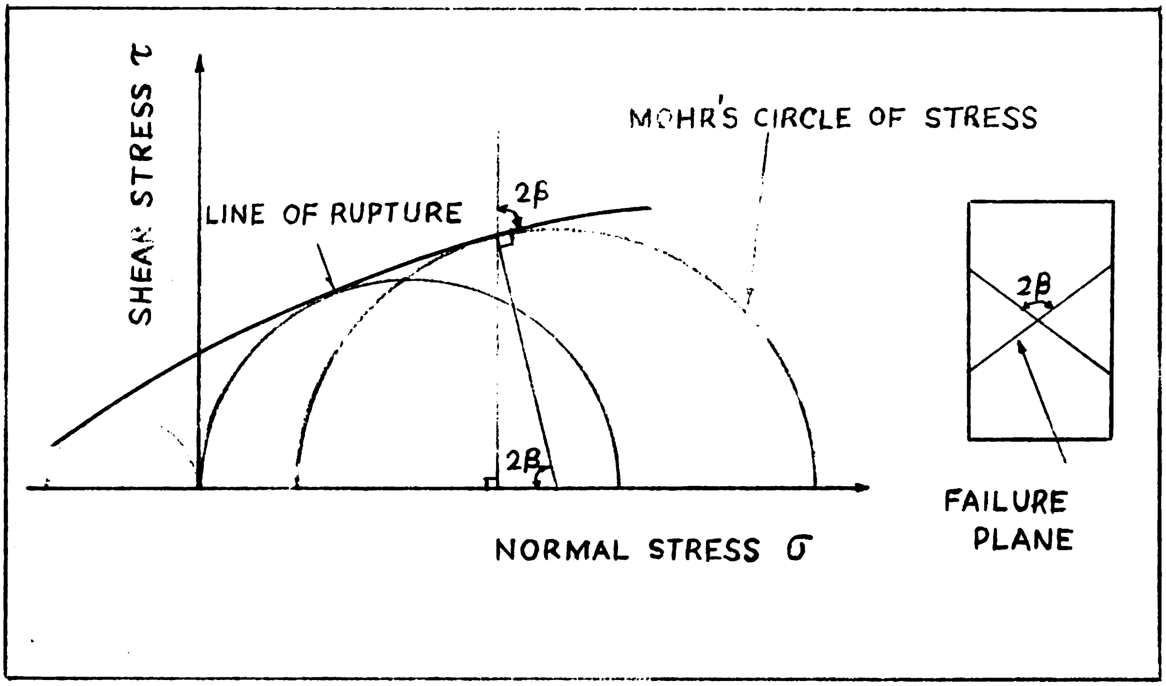

Fig. 1. Mohr's Diagram and Inclination of Failure Plane

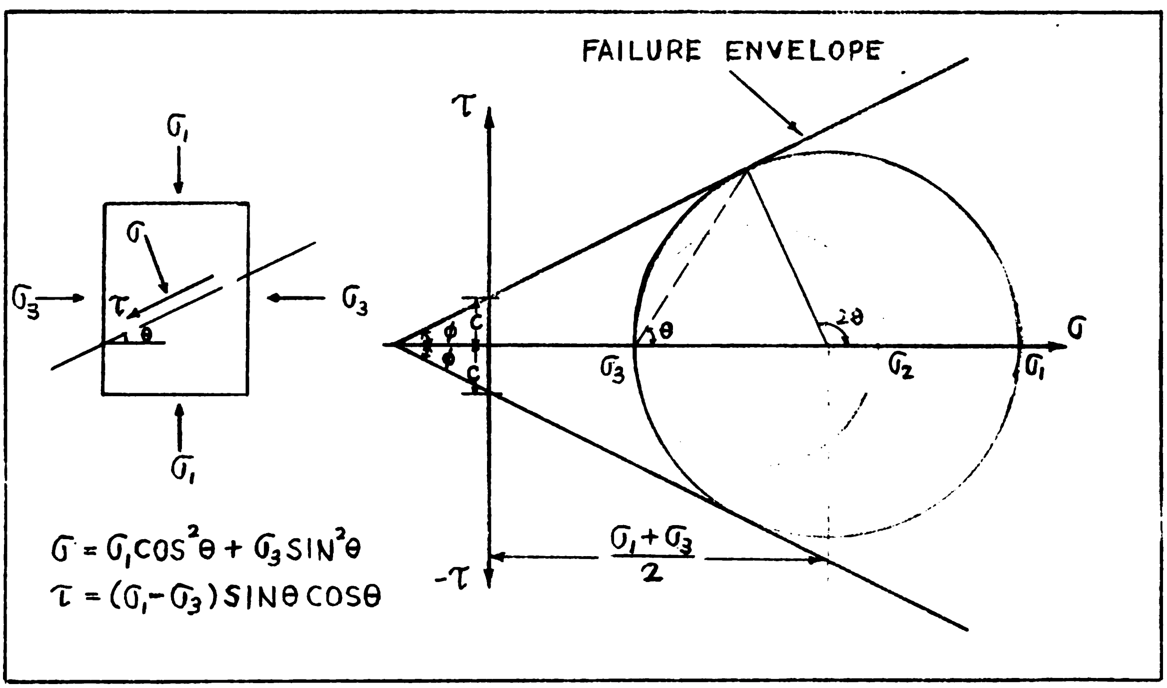

Fig. 2. Mohr's Envelope for Coulomb's Criterion

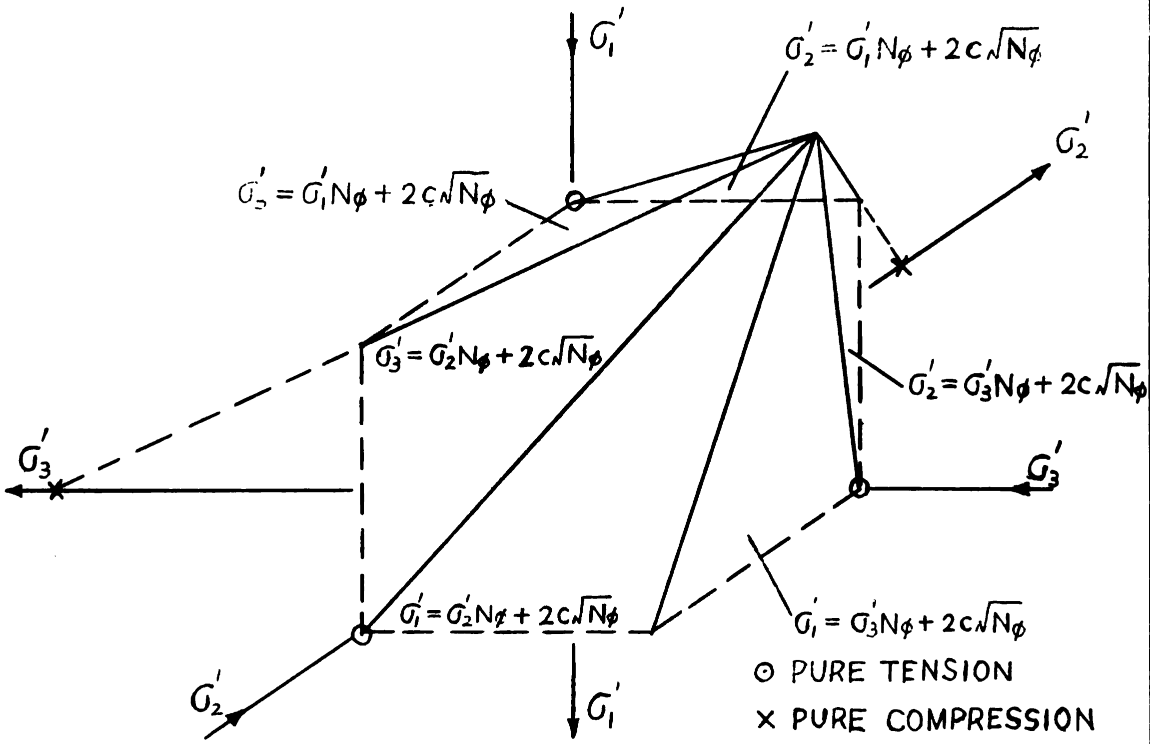

Fig. 3. Yield Surface in Principal Stress Space

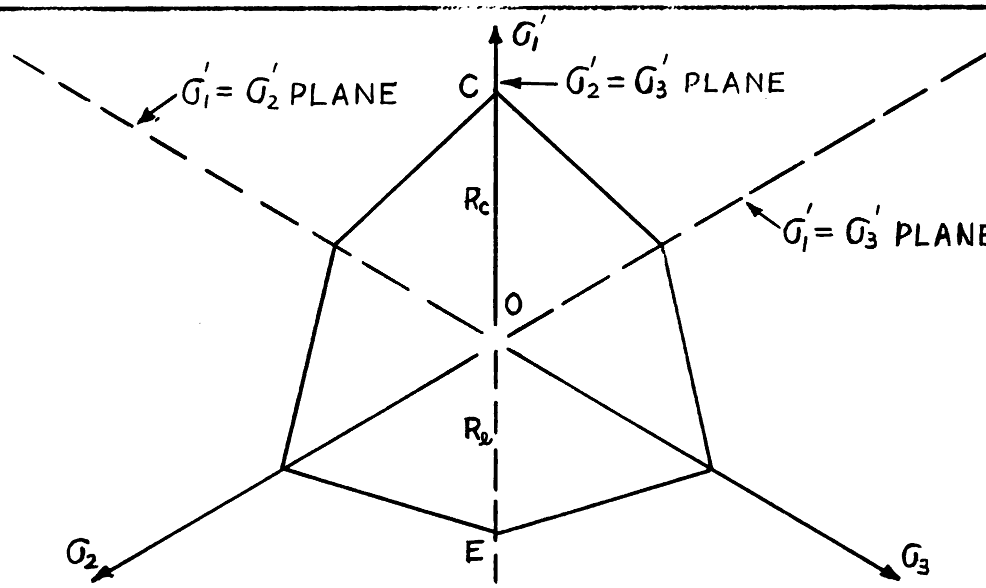

Fig. 4A. Right Section of Yield Surface by the Plane $\sigma'_1 + \sigma'_2 + \sigma'_3 = 0$

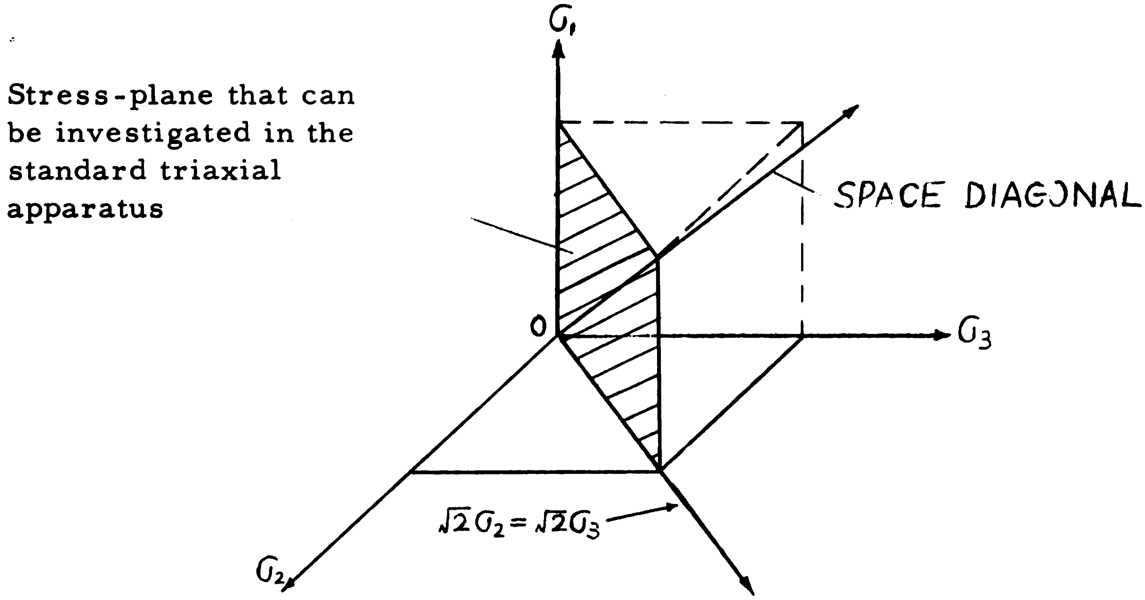

Fig. 4B. The Stress System in the Standard Triaxial Test

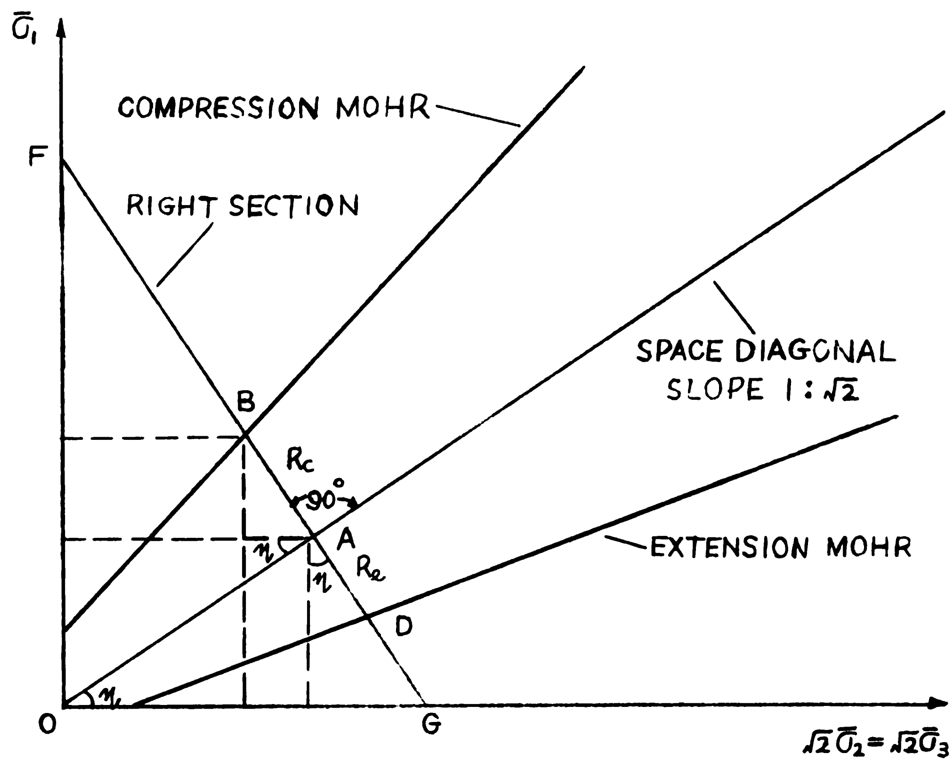

Fig. 4C. Failure Envelopes and the Stress Plane for Axially-Symmetrical Stresses

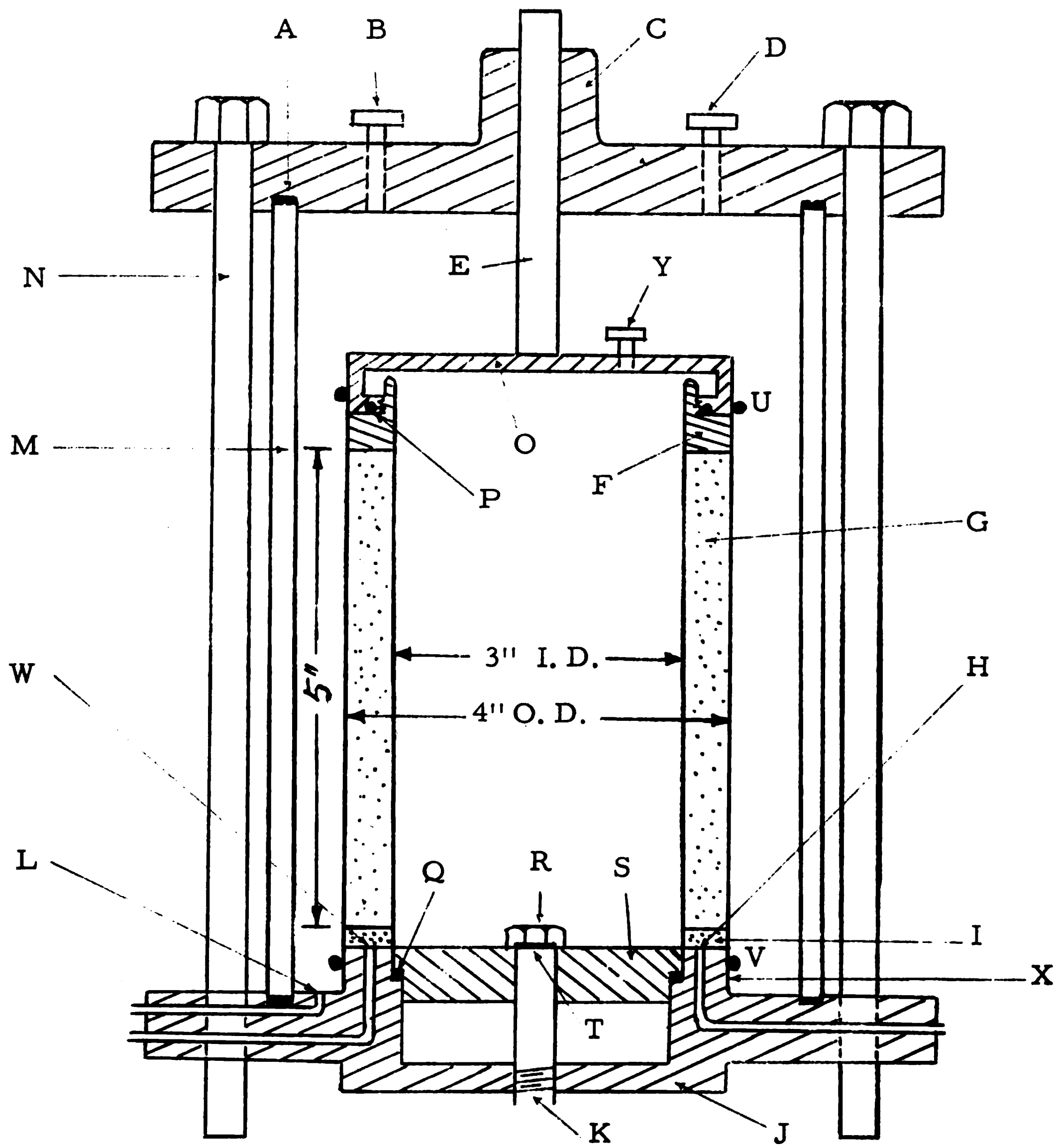

A, P, Q, T-gaskets	H-drainage	O-sealing cap
B-oil filler valve	I-porous stone	R-tightening nut
C-top cap	J-base	S-base adaptor
D-air release valve	K-bore chamber	U, V- O rings
E-loading ram	L-outside chamber	W-pore pressure
F-sample end-piece	M-pressure cylinder	X-pedestal
G-sample	N-steel tie bar	Y-air release valve

Fig. 5. Hollow Cylinder Triaxial Cell

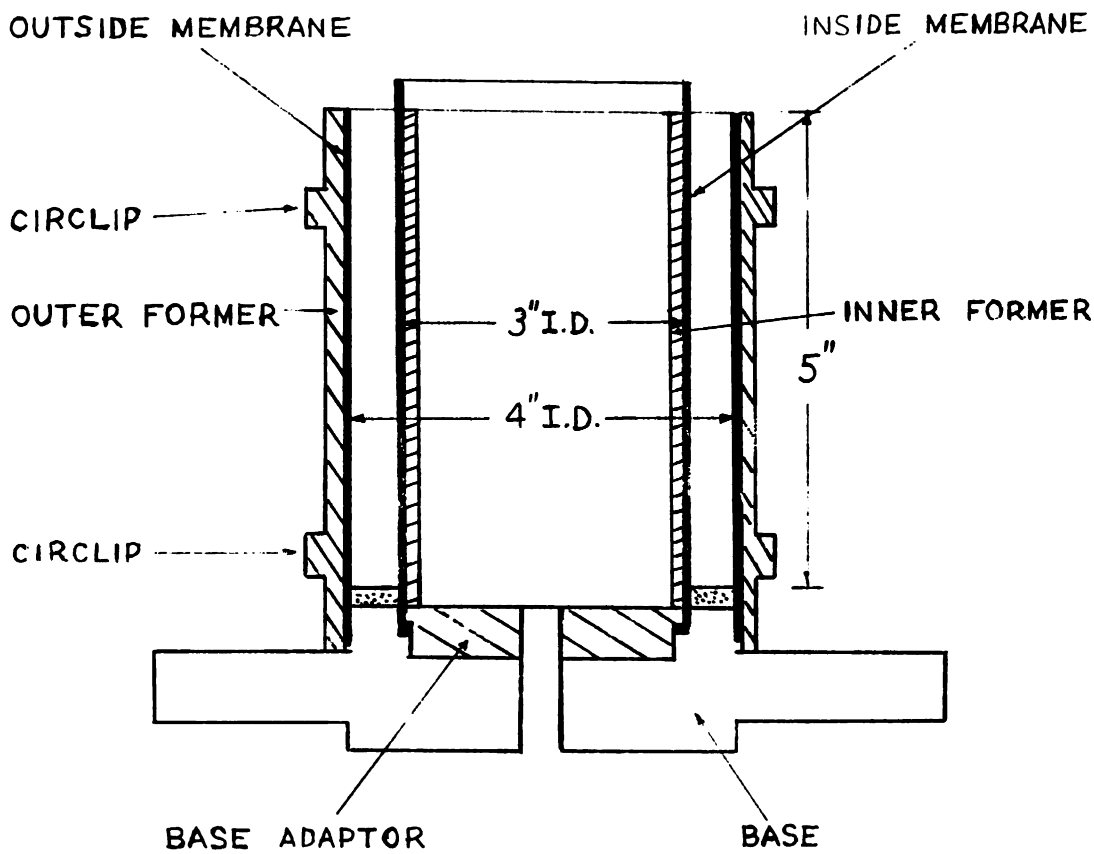

Fig. 6. The Formers for Preparing Hollow Cylindrical Specimens

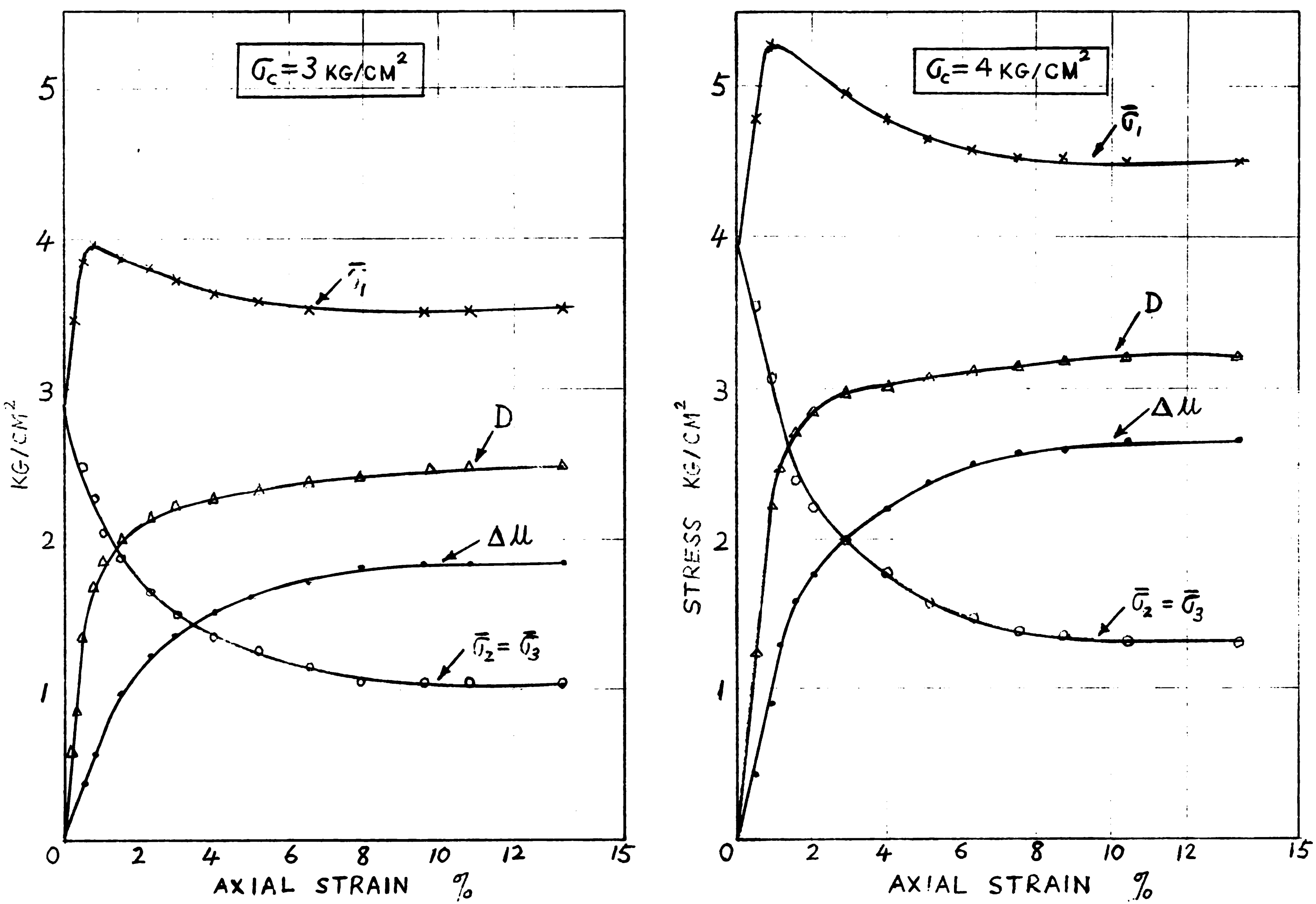

Fig. 7. Results from UCl Tests

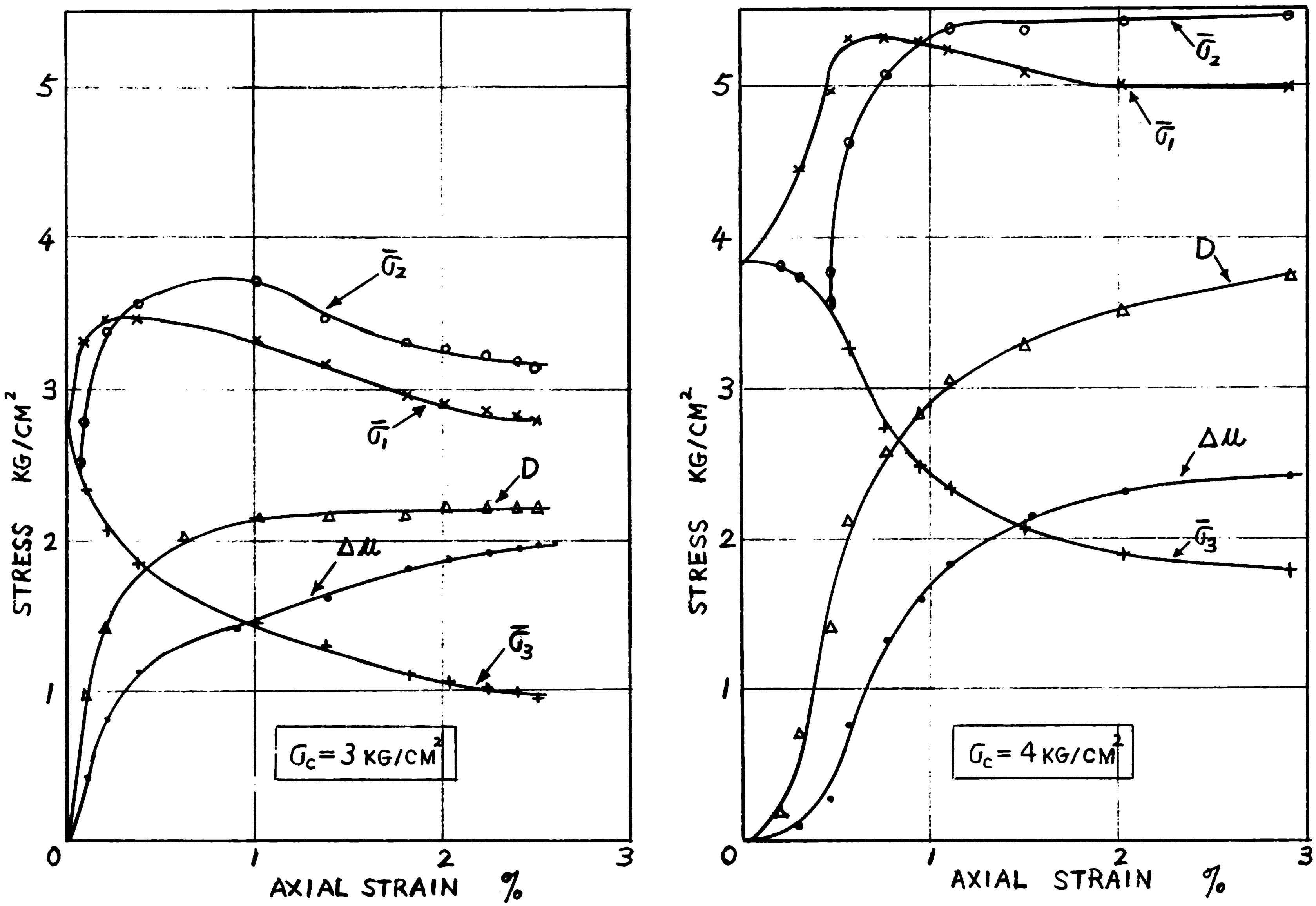

Fig. 8. Results from U11 Tests

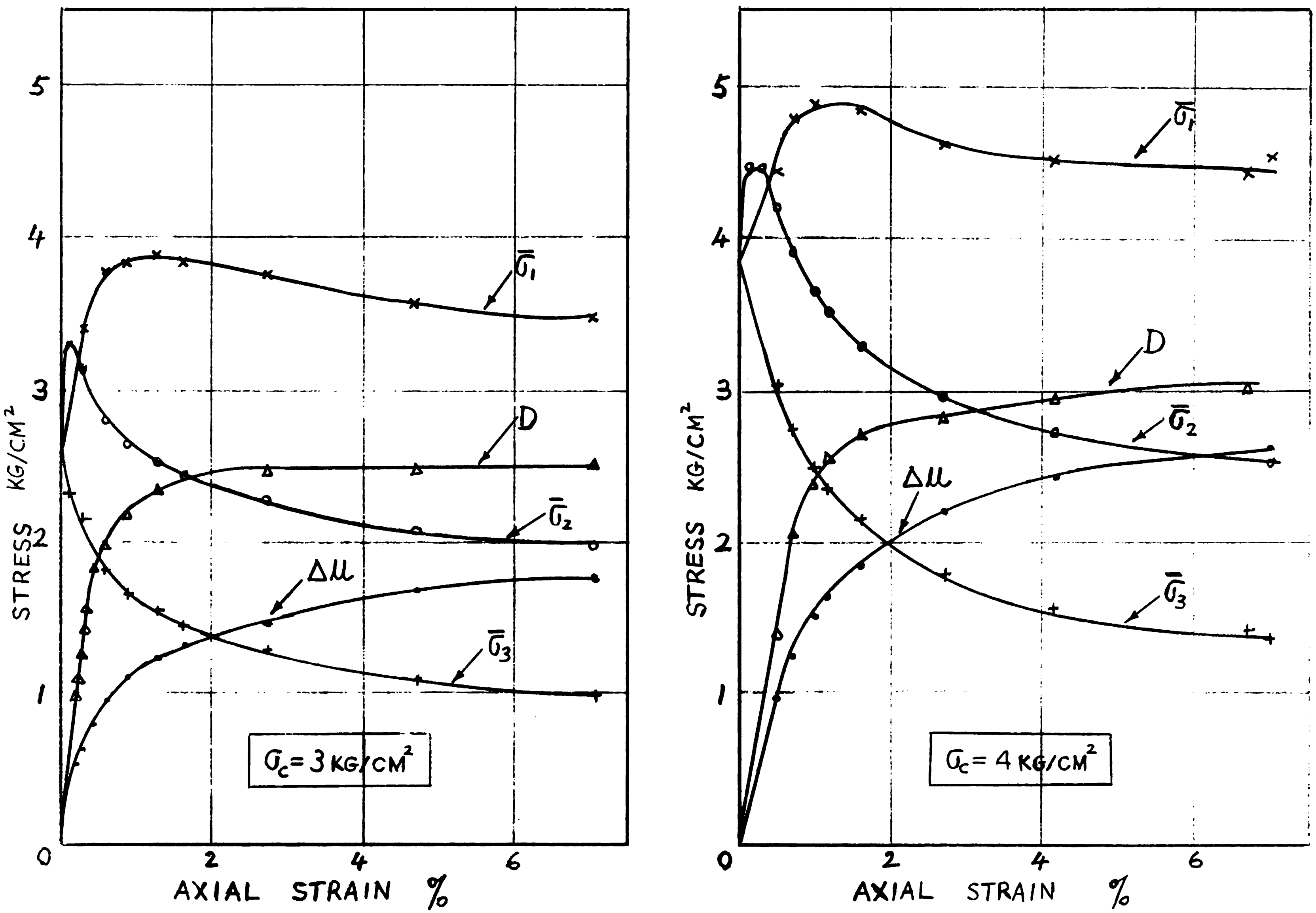

Fig. 9. Results from UI2 Tests

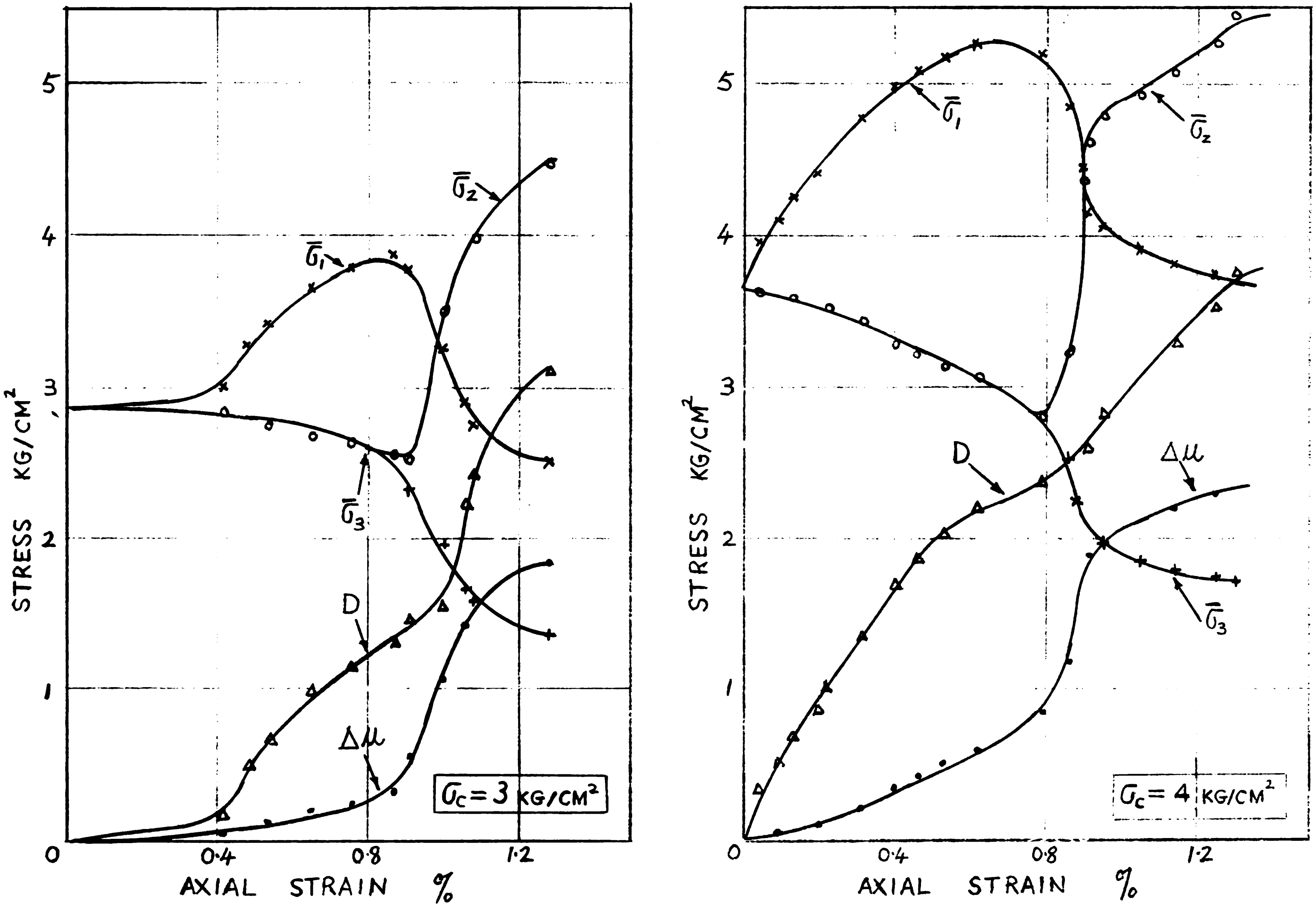

Fig. 10. Results from UI3 Tests

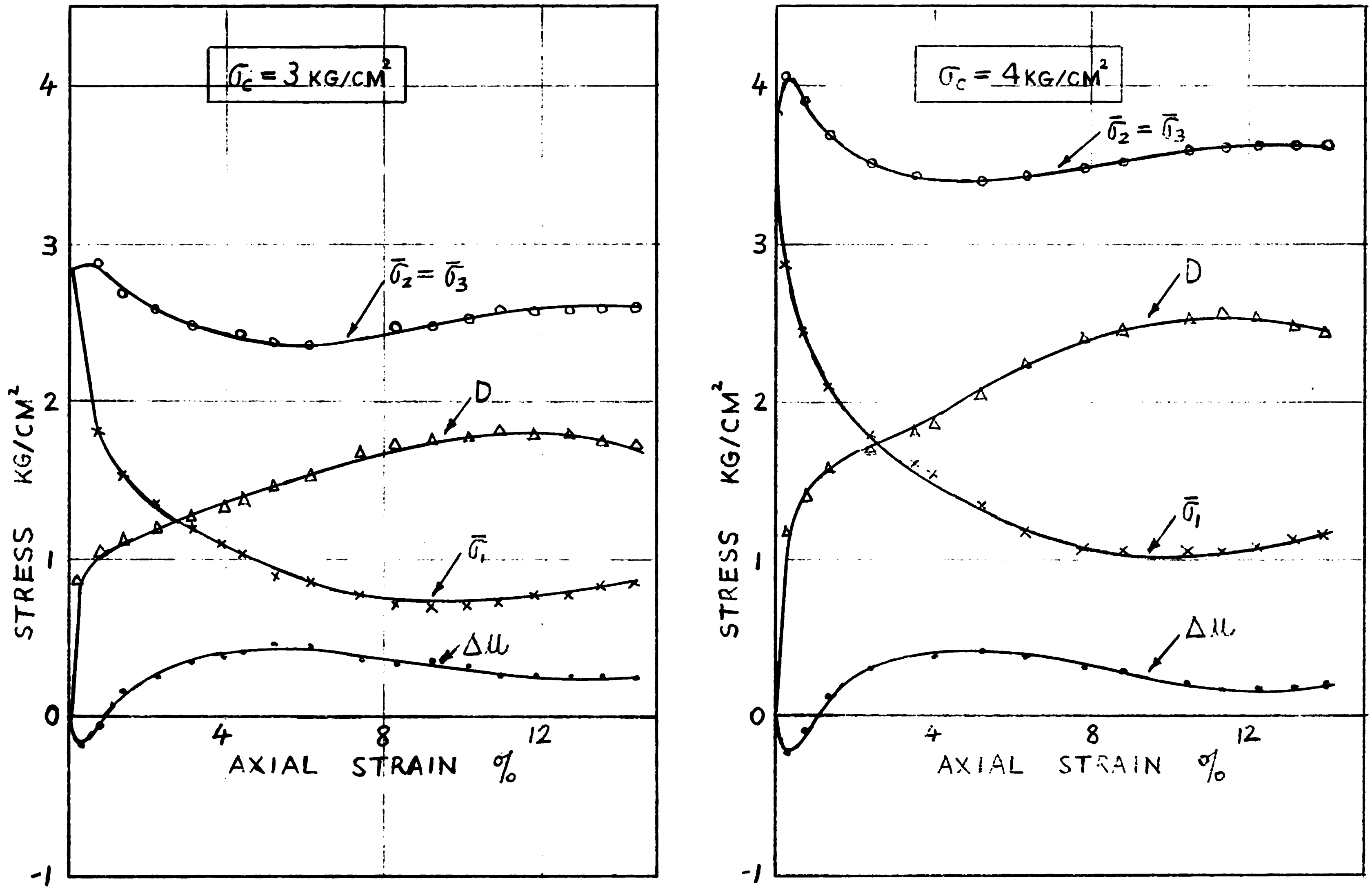

Fig. 11. Results from UEl Tests

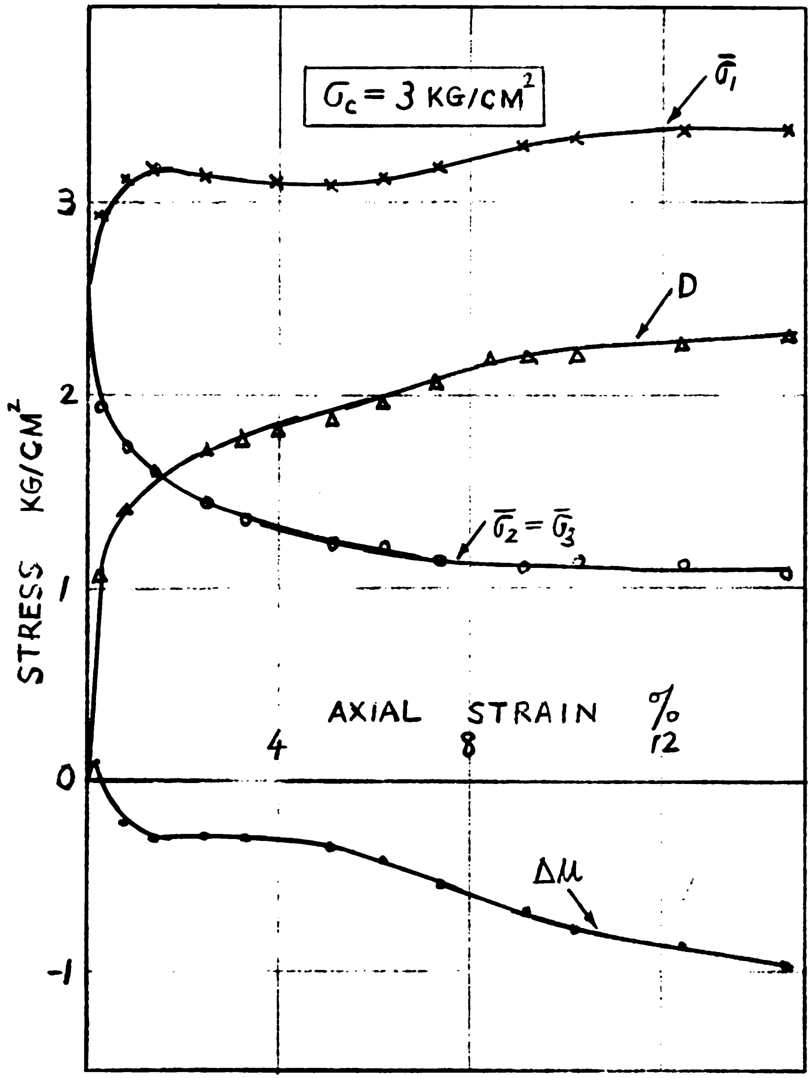

Fig. 12. Results from UC2 Test

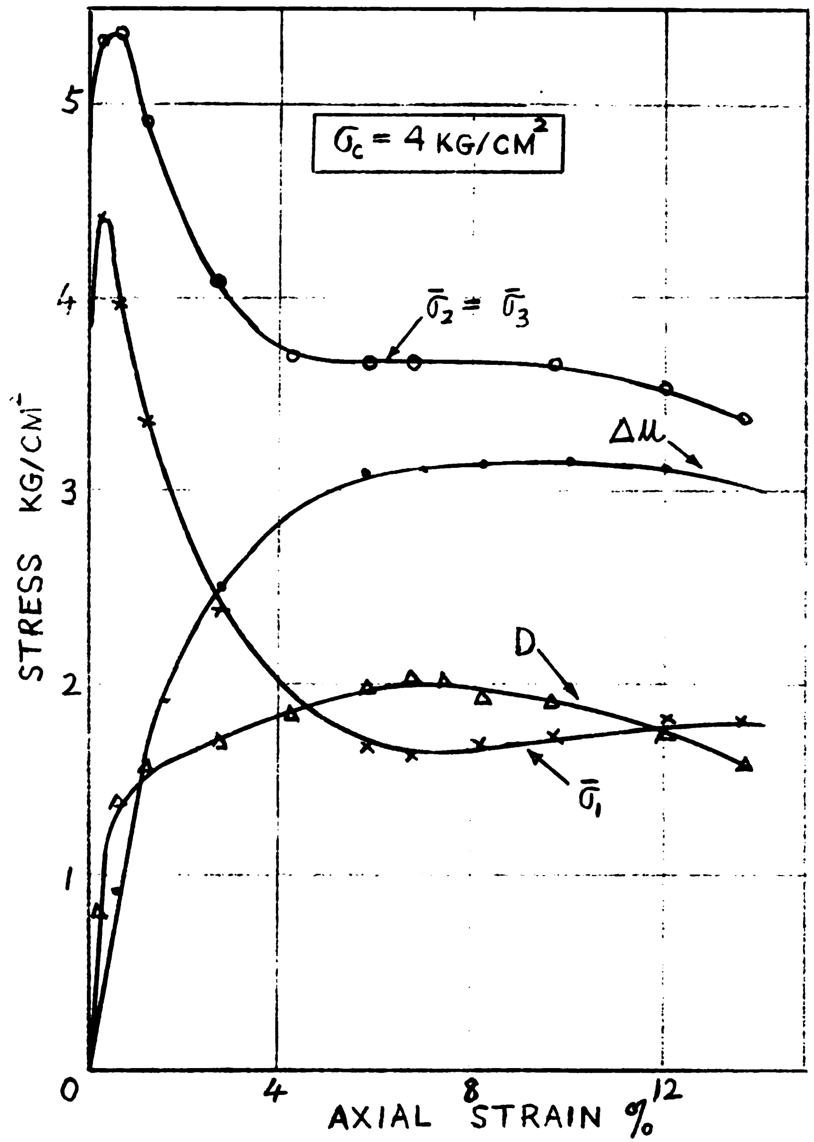

Fig. 13. Results from UE2 Test

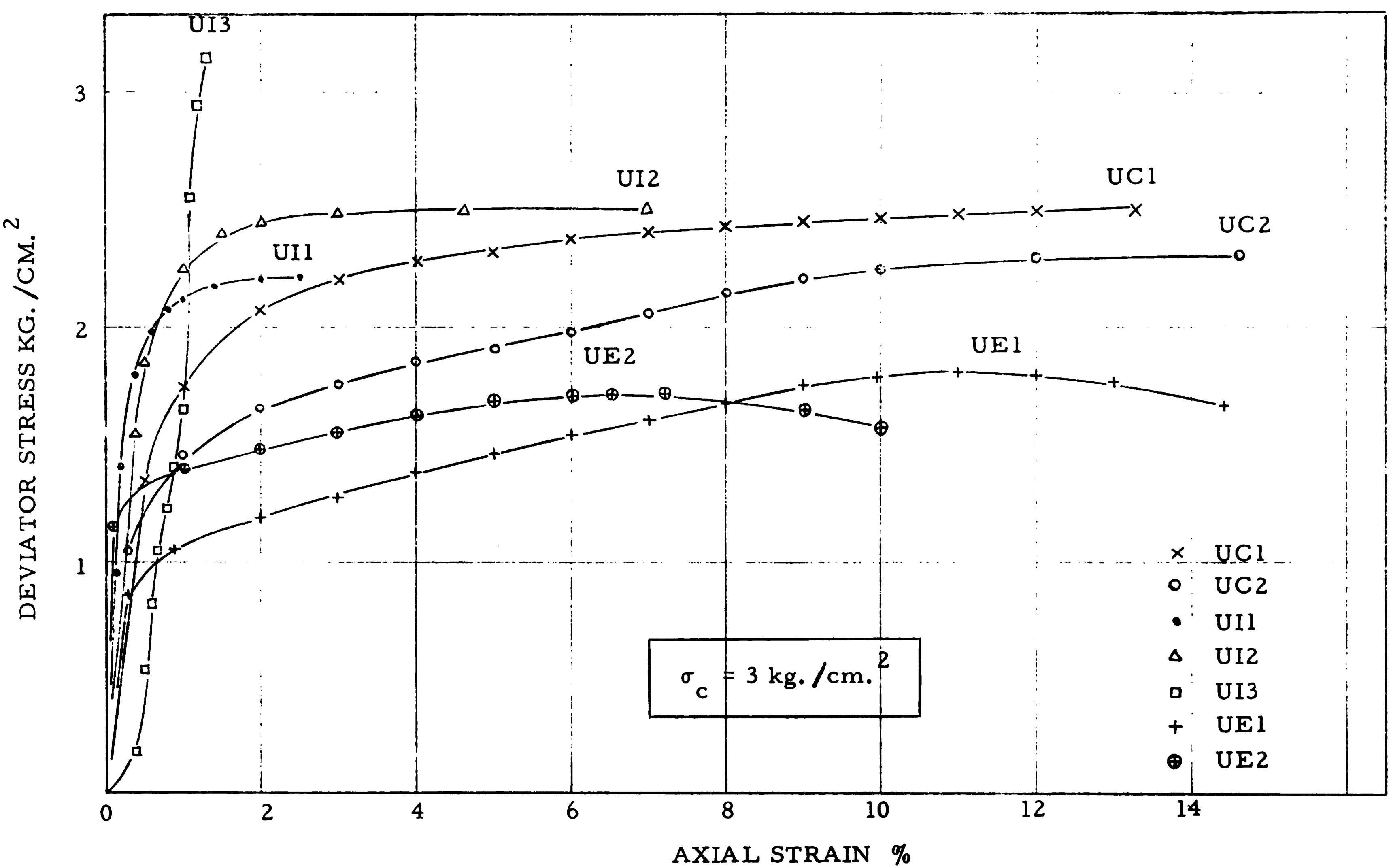

Fig. 14. Summary of Deviator Stress vs. Strain Curves for Tests at $\sigma_c = 3$ kg. /cm.^{2}

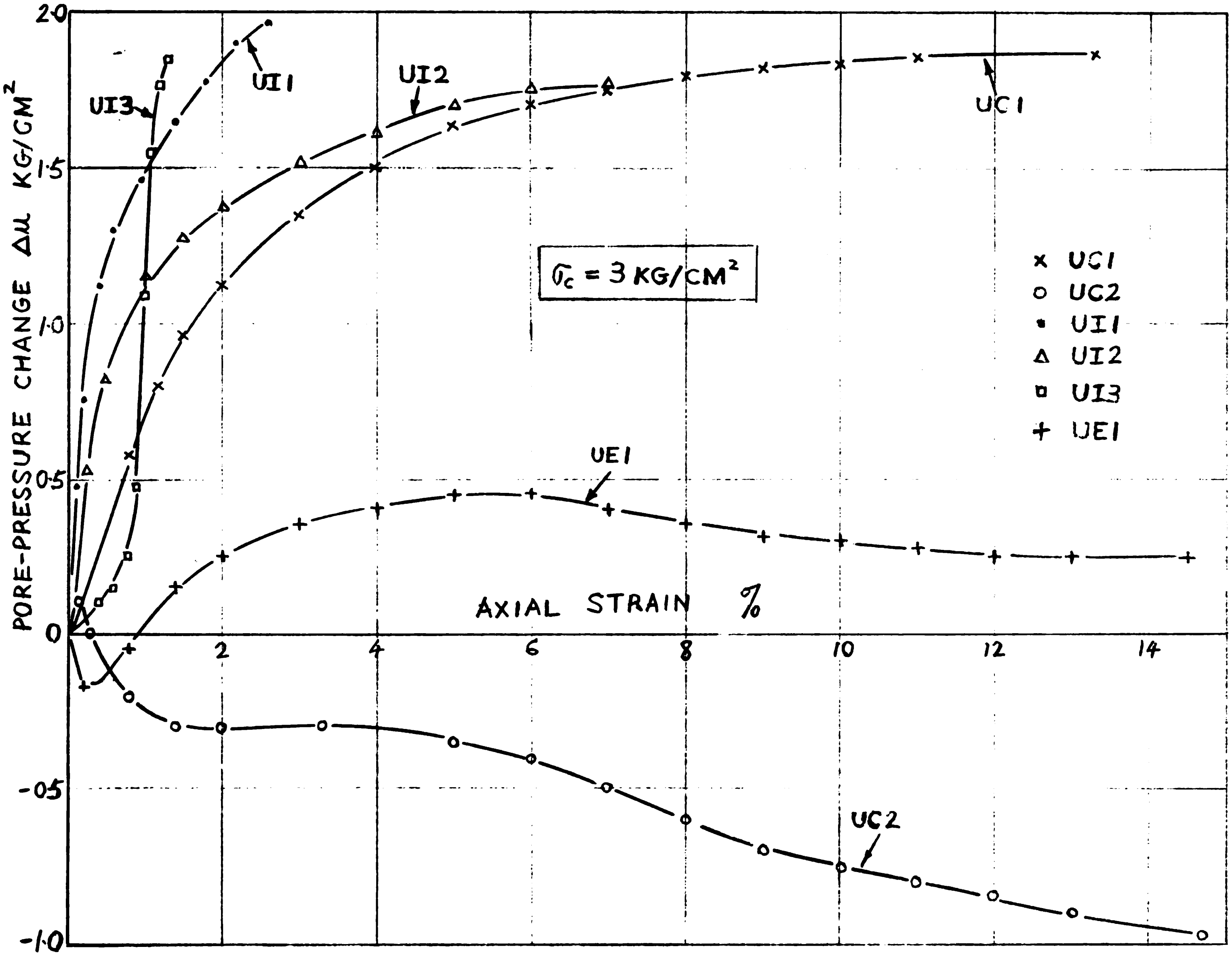

Fig. 15A. Summary of Pore-pressure vs. Strain Curves for Tests at $\sigma_c = 3$ kg./cm.^{2}

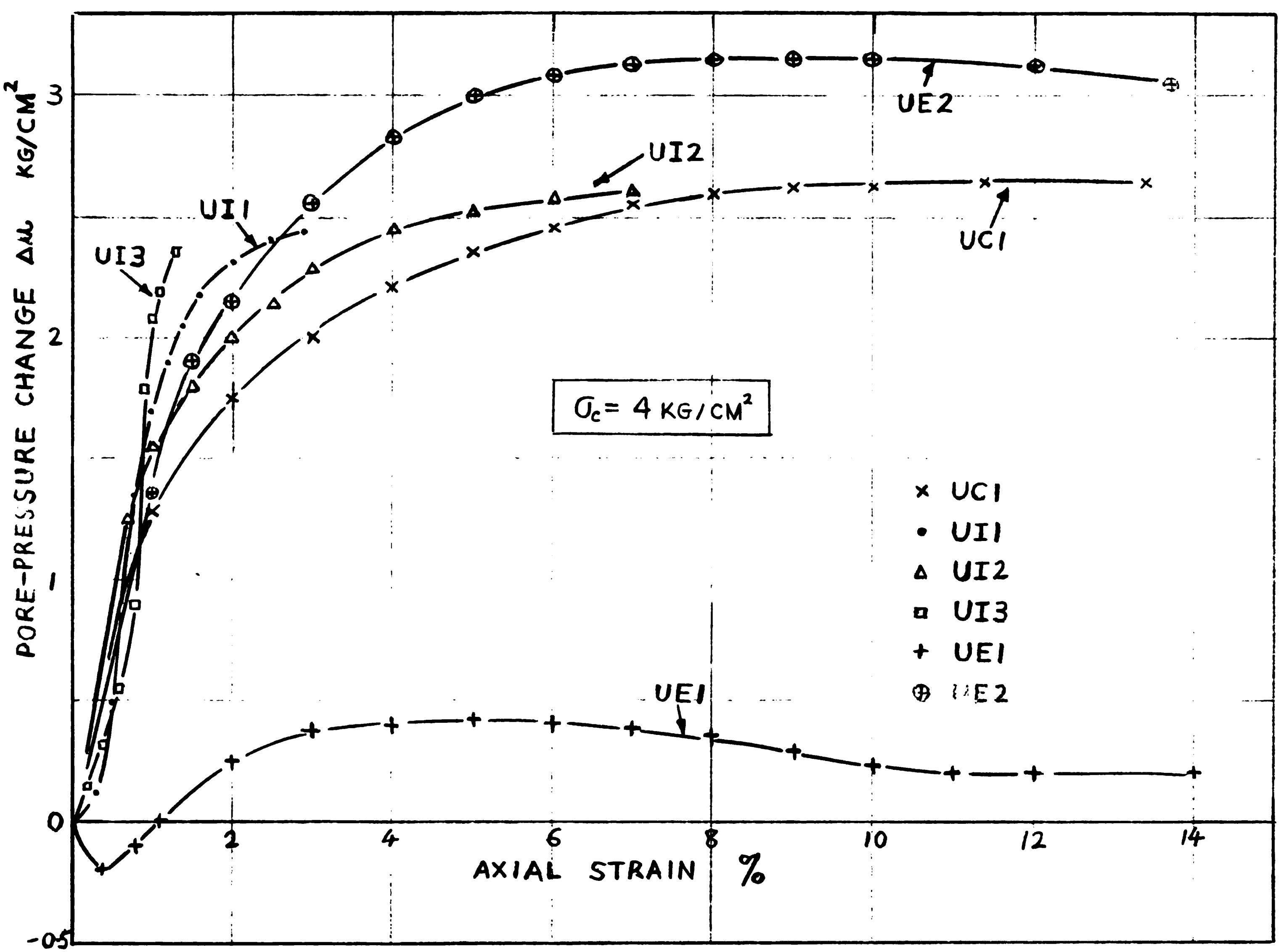

Fig. 15B. Summary of Pore-pressure vs. Strain Curves for Tests at σ_c = 4 kg./cm.^{2}

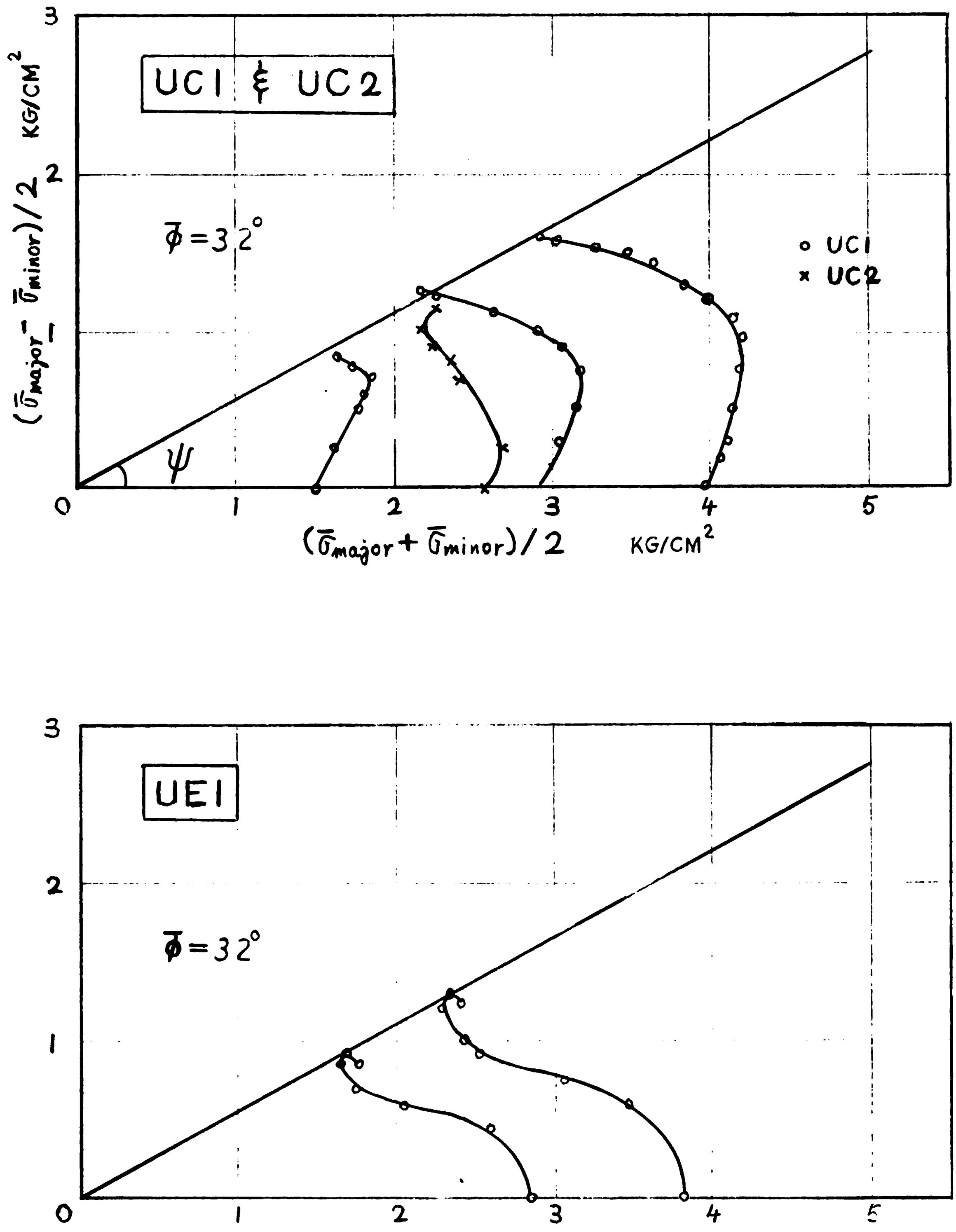

Fig. 16A. Mohr's Effective Stress Failure Envelopes and Stress Paths

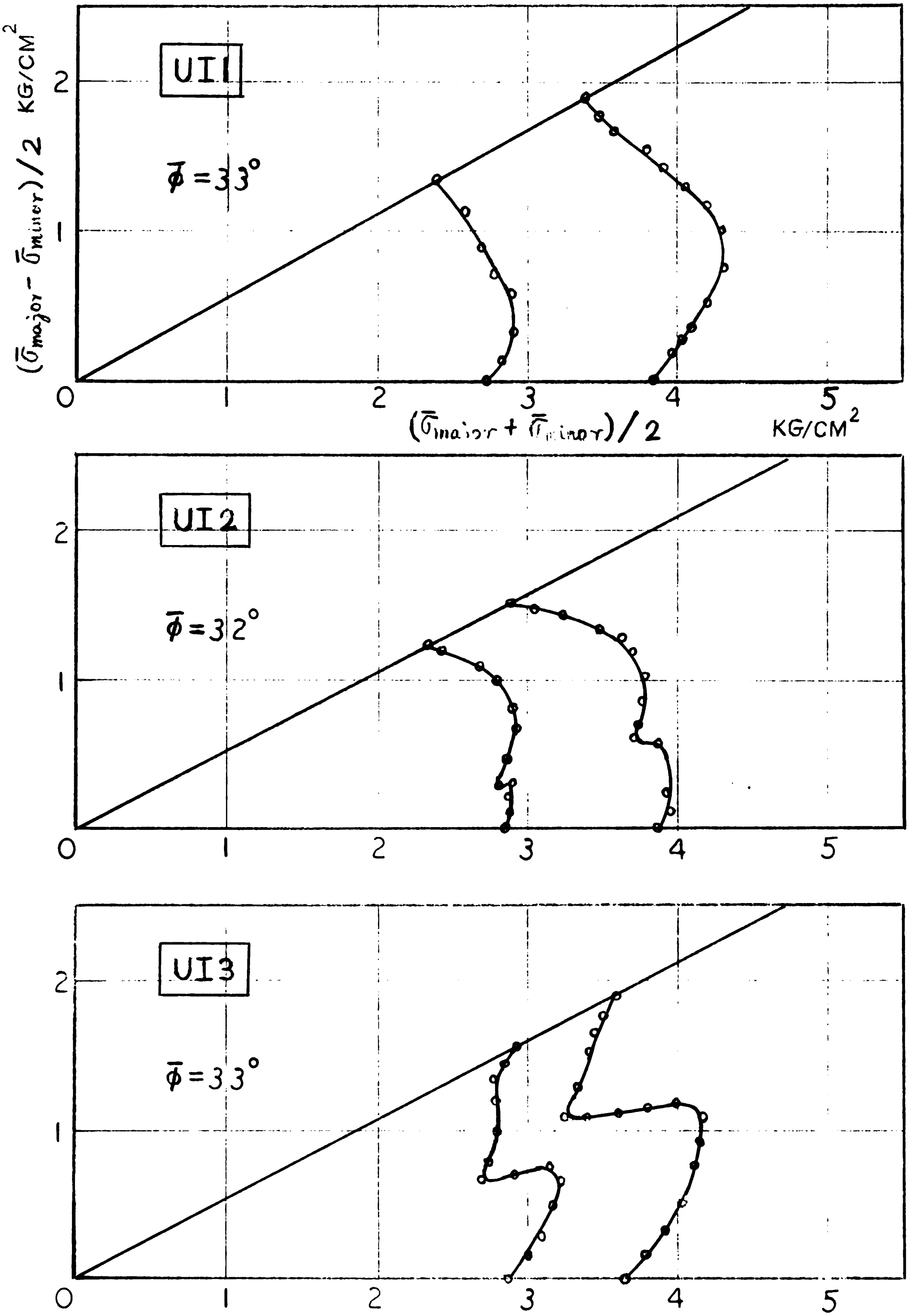

Fig. 16B. Mohr's Effective Stress Failure Envelopes and Stress Paths

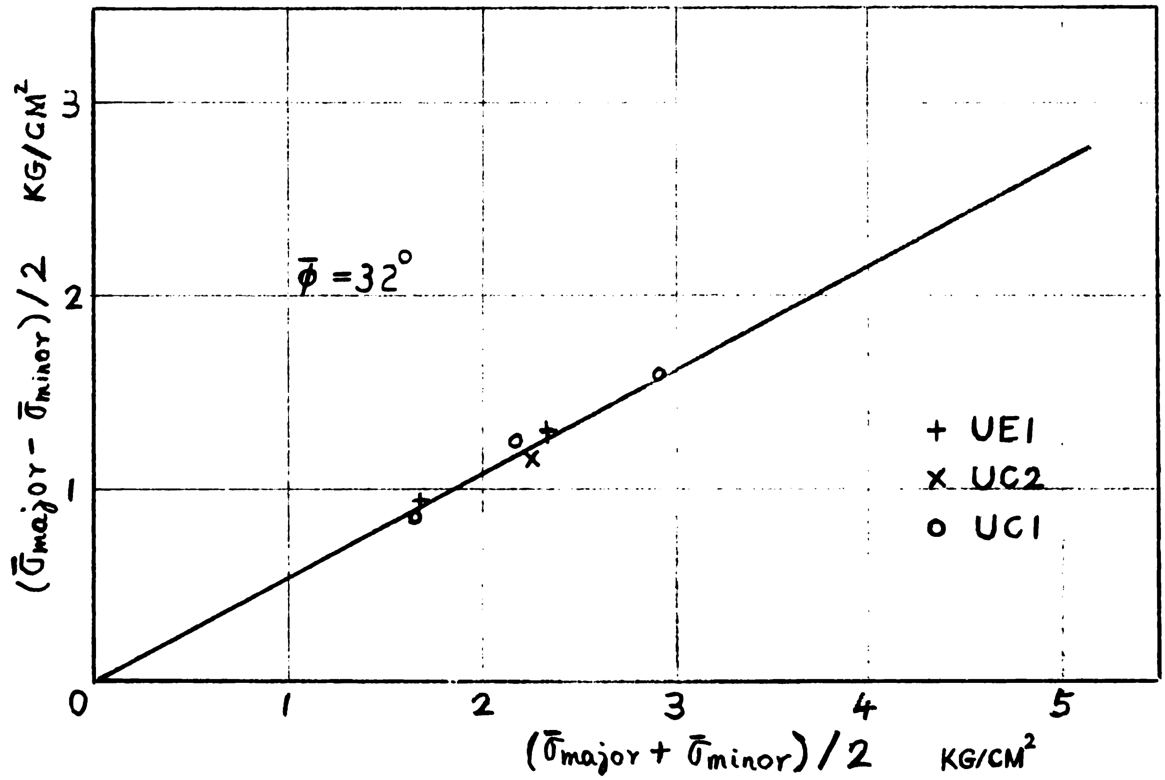

Fig. 17A. Mohr's Failure Envelope from UC1, UC2 and UE1 Tests

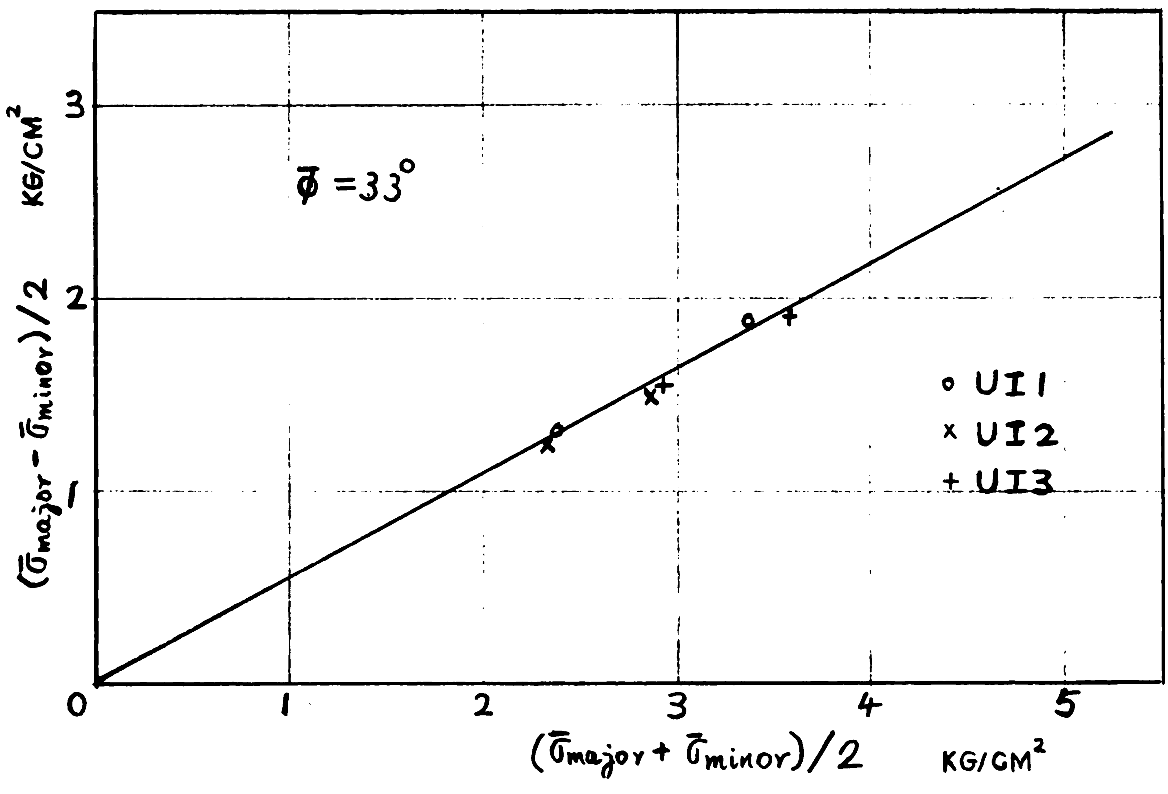

Fig. 17B. Mohr's Failure Envelopes from UI1, UI2, and UI3 Tests

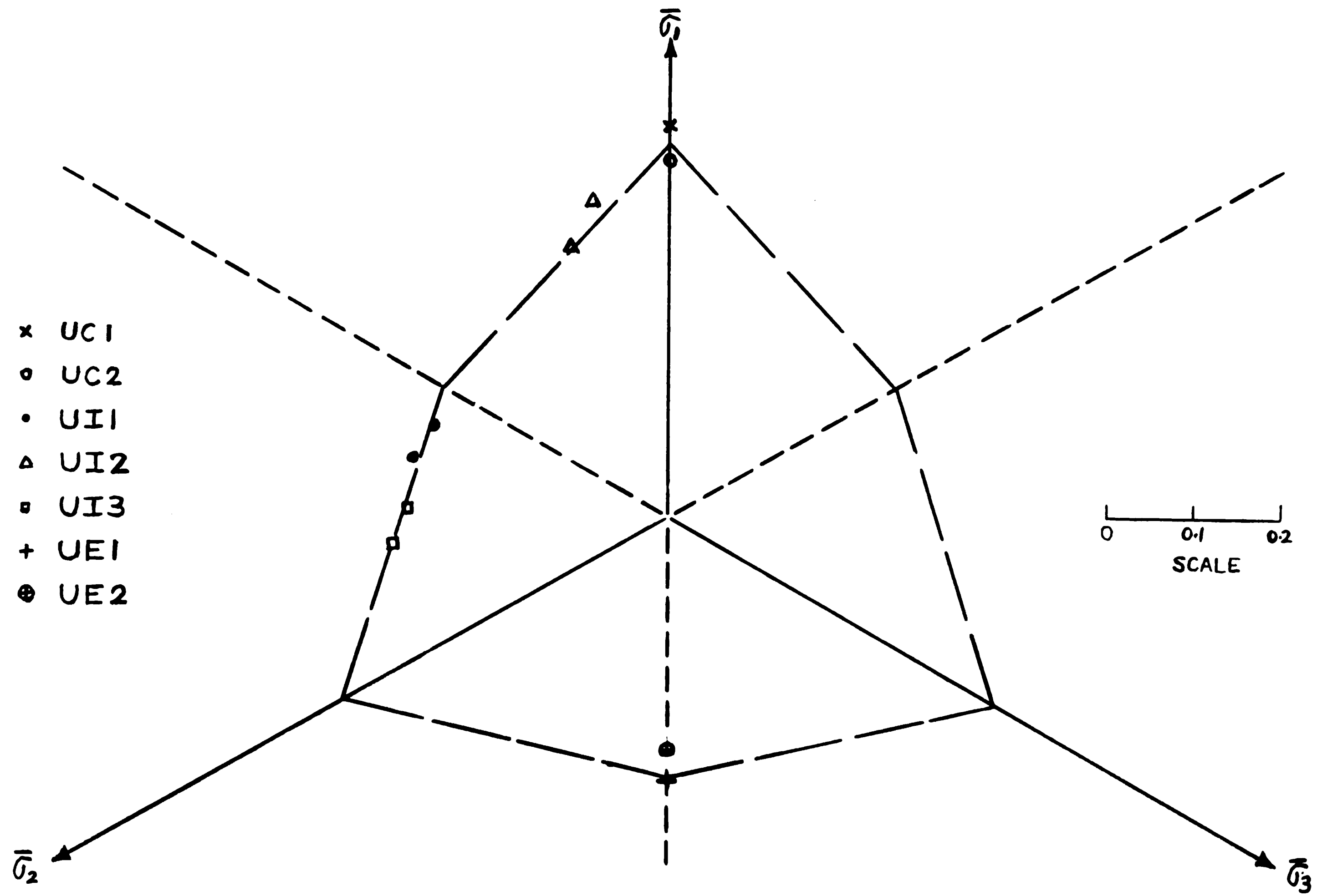

Fig. 18. Failure Surface in Effective Principal Stress Space Projection onto the Plane $\sigma''_1 + \sigma''_2 + \sigma''_3 = 1$. Coulomb's Criterion for $\bar{c} = 0$, $\phi = 32^o$ is shown as dotted lines.

Table 6. Details of failure conditions

Test	Consol. σ_c kg./cm.^{2}	$\bar{\sigma}_{1f}$ kg./cm.^{2}	$\bar{\sigma}_{2f}$ kg./cm.^{2}	$\bar{\sigma}_{3f}$ kg./cm.^{2}	Max D_f kg./cm.^{2}	$(\Delta u)_f$ kg./cm.^{2}	Axial strain ϵ_f %	Water content w_f %	Mode of failure
UC1	3.0 4.0	3.53 4.54	1.03 1.31	1.03 1.31	2.50 3.23	+1.84 +2.65	13.30 13.40	29.3 28.2	Bulging in center
UC2	3.0	3.37	1.08	1.08	2.15	-0.98	14.60	27.6	Bulging in center
UI1	3.0 4.0	2.98 4.99	3.71 5.54	1.05 1.79	2.66 3.75	+1.97 +2.44	2.5+ 2.90	29.5 28.6	Curved shear surfaces in neighborhood of center
UI2	3.0 3.0 4.0	3.48 3.49 4.55	1.58 1.98 2.54	0.935 0.985 1.36	2.54 2.56 3.19	+1.98 +1.82 +2.58	7.68 7.50 7.0	29.1 29.5 28.7	Curved shear surfaces in neighborhood of center
UI3	3.0 4.0	2.51 3.69	4.48 5.46	1.37 1.71	3.11 3.75	+1.84 +2.34	1.28 1.30	30.0 28.1	Vertical shear cracks followed by curved shear surfaces
UE1	3.0 4.0	0.75 1.07	2.58 3.60	2.58 3.60	1.83 2.53	+0.27 +0.28	10.90 10.40	27.0 26.1	"Necking" preceded by curved shear surfaces at top and bottom of sample
UE2	4.0	1.70	3.76	3.76	2.06	+3.08	7.0	26.1	"Necking" preceded by curved shear surfaces at top and bottom of specimen

Table 7. Stress conditions at failure

Test	σ_c kg./cm.^{2}	$\frac{\bar{\sigma}_1}{\sigma_c}$	$\frac{\bar{\sigma}_2}{\sigma_c}$	$\frac{\bar{\sigma}_3}{\sigma_c}$	$\bar{p}=\frac{1}{3}(\bar{\sigma}_1+\bar{\sigma}_2+\bar{\sigma}_3) \times \frac{1}{\sigma_c}$	$\frac{D}{\sigma_c}$	$(\bar{\sigma}\text{ major} + \bar{\sigma}\text{ minor}) \times \frac{1}{\sigma_c}$	$\frac{\bar{\sigma}\text{ major}}{\bar{\sigma}\text{ minor}}$	$\frac{D}{\bar{p}} \times \frac{1}{\sigma_c}$	$\frac{\Delta u}{\sigma_c}$
UC1	3.0	1.18	0.34	0.34	0.62	0.834	1.52	3.47	1.35	0.613
	4.0	1.14	0.33	0.33	0.60	0.808	1.46	3.46	1.35	0.662
UC2	3.0	1.12	0.36	0.36	0.62	0.715	1.48	3.11	1.16	-0.326
UI1	3.0	0.98	1.24	0.35	0.86	0.89	1.59	3.54	1.03	0.65
	4.0	1.25	1.39	0.45	1.03	0.94	1.83	3.09	0.91	0.61
UI2	3.0	1.16	0.53	0.31	0.67	0.85	1.47	3.74	1.27	0.66
	3.0	1.16	0.66	0.33	0.72	0.85	1.49	3.52	1.18	0.605
	4.0	1.14	0.64	0.34	0.71	0.80	1.48	3.35	1.13	0.645
UI3	3.0	0.84	1.49	0.46	0.93	1.04	1.95	3.24	1.12	0.613
	4.0	0.92	1.37	0.42	0.90	0.94	1.79	3.26	1.04	0.585
UE1	3.0	0.25	0.86	0.86	0.66	0.61	1.11	3.44	0.93	0.09
	4.0	0.27	0.90	0.90	0.69	0.63	1.17	3.34	0.91	0.07
UE2	4.0	0.43	0.94	0.94	0.77	0.52	1.37	2.18	0.67	0.77

Table 8. Comparison of stress conditions at failure for Michigan clay and Weald clay

Test	$\frac{\bar{\sigma}_1}{\sigma_c}$	$\frac{\bar{\sigma}_2}{\sigma_c}$	$\frac{\bar{\sigma}_3}{\sigma_c}$	$\bar{p} = \frac{1}{3}(\bar{\sigma}_1+\bar{\sigma}_2+\bar{\sigma}_3) \times 1/\sigma_c$	$\frac{D}{\sigma_c}$	$\frac{(\bar{\sigma}\text{ major}}{+\bar{\sigma}\text{ minor})} \times \frac{1}{\sigma_c}$	$\frac{(\bar{\sigma}\text{ major}}{\bar{\sigma}\text{ minor}}$	$\frac{D}{\bar{p}} \times \frac{1}{\sigma_c}$	$\frac{\Delta u}{\sigma_c}$
UC1	1.16	0.34	0.34	0.61	0.82	1.49	3.47	1.35	0.64
UC2	1.12	0.36	0.36	0.62	0.72	1.48	3.11	1.16	-0.33
UI1	1.12	1.31	0.40	0.95	0.91	1.71	3.32	0.97	0.63
UI2	1.15	0.61	0.33	0.70	0.83	1.48	3.54	1.19	0.63
UI3	0.88	1.43	0.44	0.92	0.99	1.87	3.25	1.08	0.40
UE1	0.26	0.88	0.88	0.67	0.62	1.14	3.39	0.92	0.08
UE2	0.43	0.94	0.94	0.77	0.52	1.37	2.18	0.67	0.77
Weald Clay, N.C. (PARRY, 1960):									
1. Compression									
a. $\sigma_2=\sigma_3=$const.	1.04	0.46	0.46	0.65	0.58	1.50	2.26	0.89	0.54
b. σ_1 = constant	0.96	0.45	0.45	0.62	0.51	1.41	2.13	0.82	-0.03
2. Extension									
a. $\sigma_2=\sigma_3=$const.	0.40	0.87	0.87	0.71	0.47	1.26	2.19	0.67	0.13
b. σ_1=constant	0.38	0.87	0.87	0.71	0.49	1.25	2.32	0.70	0.62

Table 9. Summary of effective strength parameters from consolidated undrained triaxial tests on Michigan clay

Test	$\bar{c}$	$\bar{\phi}$
UC1, UC2	0	32°
UE1	0	32°
UI1	0	33°
UI 2	0	32°
UI3	0	33°
UC1, UC2, UE1	0	32°
UI1, UI2, UI3	0	33°

Table 10. Coordinates in effective principal stress space of experimental stress points on the plane $\sigma''_1+\sigma''_2+\sigma''_3=1$

Test	σ_c kg./cm.^{2}	$\bar{\sigma}_{1f}$ kg./cm.^{2}	$\bar{\sigma}_{2f}$ kg./cm.^{2}	$\bar{\sigma}_{3f}$ kg./cm.^{2}	$(\bar{\sigma}_{1f}+\bar{\sigma}_{2f}+\bar{\sigma}_{3f})$ kg./cm.^{2}	$\sigma''_1 = \frac{\bar{\sigma}_{1f}}{(\bar{\sigma}_{1f}+\bar{\sigma}_{2f}+\bar{\sigma}_{3f})}$	$\sigma''_2 = \frac{\bar{\sigma}_{2f}}{(\bar{\sigma}_{1f}+\bar{\sigma}_{2f}+\bar{\sigma}_{3f})}$	$\sigma''_3 = \frac{\bar{\sigma}_{3f}}{(\bar{\sigma}_{1f}+\bar{\sigma}_{2f}+\bar{\sigma}_{3f})}$
UC1	3.0	3.53	1.03	1.03	5.59	0.631	0.184	0.184
	4.0	4.54	1.31	1.31	7.16	0.634	0.183	0.183
UC2	3.0	3.37	1.08	1.08	5.53	0.61	0.195	0.195
UI1	3.0	2.98	3.71	1.05	7.74	0.385	0.48	0.149
	4.0	4.99	5.54	1.79	12.32	0.405	0.449	0.145
UI2	3.0	3.48	1.58	0.935	6.0	0.58	0.264	0.156
	3.0	3.49	1.98	0.985	6.46	0.54	0.306	0.152
	4.0	4.55	2.54	1.36	8.45	0.54	0.301	0.161
UI3	3.0	2.51	4.48	1.37	8.36	0.30	0.535	0.164
	4.0	3.69	5.46	1.71	10.86	0.34	0.503	0.158
UE1	3.0	0.75	2.58	2.58	5.91	0.127	0.435	0.435
	4.0	1.07	3.60	3.60	8.27	0.130	0.435	0.435
UE2	4.0	1.70	3.76	3.76	9.22	0.184	0.408	0.408

BIBLIOGRAPHY

ANDRESEN, A. and SIMONS, N. E., 1960. Norwegian triaxial equipment and technique, Norwegian Geotechnical Institute, Publication No. 35.

BISHOP, A. W. and ELDIN, A. K. GAMAL, 1953. The effect of stress history on the relation between ϕ and porosity in sand. Proc. 3rd Int. Conf. Soil Mech., 1 : 100.

BISHOP, A. W. and HENKEL, D. J., 1957. The measurement of soil properties in the triaxial test, Edward Arnold, London.

DRUCKER, D. C., 1953. Limit analysis of two- and three-dimensional soil mechanic problems. J. Mech. Phys. Solids, 1 : 4 : 217.

HABIB, P., 1953. Influence de la variation de la contrainte principale moyenne sur la résistance au cisaillement des sols. Proc. 3rd Int. Conf. Soil Mech., 1 : 131.

HAYTHORNTHWAITE, R. M., 1960a. Mechanics of the triaxial test for soils, Proc. A. S. C. E., Vol. 86, SM5.

HAYTHORNTHWAITE, R. M., 1960b. Stress and strain in soils, Plasticity, Proc. 2nd Symposium on Naval Structural Mechanics, Pergamon Press.

HENKEL, D. J., 1959. The relationships between the strength, pore-pressure, and volume-change characteristics of saturated clays, Geotechnique, 9 : 3 : 119.

HENKEL, D. J., 1960. The relationships between the effective stresses and water content in saturated clays, Geotechnique, 10 : 2 : 41.

HILL, R., 1950. The mathematical theory of plasticity, Oxford Press, London.

HVORSLEV, M. J., 1960. Physical components of the shear strength of saturated clays, Proc. A. S. C. E. Research Conf. on Shear Strength of Cohesive Soils.

KIRKPATRICK, W. M., 1953. The condition of failure for sands, Proc. 3rd Int. Conf. Soil Mech., 1b : 172.

PARRY, R. H. G., 1960. Triaxial compression and extension tests on remoulded saturated clay, Geotechnique, 10 : 4 : 166.

RUTLEDGE, P. C., 1940. Theories of failure of materials applied to the shearing resistance of soils, Proc. Purdue Conf. Soil Mech. and Applications, 1940.

SHIELD, R. T., 1955. On Coulomb's law of failure in soils, J. Mech. Phys. Solids, 4 : 10.

SKEMPTON, A. W., 1954. The pore-pressure coefficients A and B, Geotechnique, 4 : 4 : 143.

TAYLOR, D. W., 1948. Fundamentals of soil mechanics, John Wiley & Sons, New York.

TERZAGHI, K., 1936. The shearing resistance of saturated soils and the angle between the planes of shear, Proc. 1st Int. Conf. Soil Mech. Vol. 1 : D-7, pp. 54-56.

TIMOSHENKO, S., 1940. Strength of materials, Macmillan, London.

WU, T. H., 1958. Geotechnical properties of Glacial Lake Clays, Proc. A.S.C.E., Vol. 84, SM3.

APPENDIX

A1. TESTING PROCEDURE

1. Sample Preparation

Bulk samples of clay were thoroughly remoulded and mixed with distilled water and left in the moist room for a few days before use. The remoulded clay was prepared at a water content of 40-45%. Hollow cylindrical samples were prepared by injecting the clay into a mould formed by two formers, described previously under "APPARATUS." Solid cylindrical samples in the standard triaxial cell were prepared by the conventional procedure described by Bishop & Henkel (1957). 1.4" in diameter and 3" in height specimens were used in the UC2 tests whereas 1. 4" in diameter and 2. 5" in height specimens were used in the UE1 and UE2 tests.

2. Consolidation

The remoulded clay sample was normally-consolidated under an all-around pressure of 3 or 4 kg./cm.^{2} The consolidation process was accelerated by using filter paper stripe side drains on solid cylindrical samples, and by using a continuous jacket of filter paper side drains on the inside of hollow cylindrical samples. It was found that 24-30 hours were required for 95-100% consolidation. After consolidation, a back pressure of 1 to 1. 5 kg. /cm.^{2} was applied to the sample through the basal porous stone, in order to eliminate the possibility of developing negative pore-pressures and to dissolve any free or entrapped air which may exist in the sample or in the testing apparatus. The back pressure was maintained for at least 10 hours before the shear test was carried out. The all-around pressure in the cell was raised the same amount simultaneously.

3. Standard Triaxial Tests

UC2, UE1 and UE2 tests were carried out in the standard triaxial cell at controlled rate of strain of 2-3% per hour (0.04 - 0.06 in. per hour).

In the UC2 and UE2 tests, the cell pressure was adjusted so that the axial stress was kept constant and equal to the initial cell pressure $(\sigma_3)_o$ by the following equation

$$\sigma_3 = \left[(\sigma_3)_o - \frac{N\delta}{a}\right]\left[\frac{1}{1 - a_r/a}\right]$$

where

σ_3 is the cell pressure at any time during the test

N is the proving ring factor expressed in load per division

δ is the proving ring deflection in div. from zero load

a_r is the area of the ram

and a is the area of the sample at any time.

The weight of the ram has been neglected in all the calculations. In order to determine rapidly the value of σ_3 required to keep the axial stress σ_1 constant at any stage, a series of curves relating all the variables was prepared before starting the test.

Some modifications on the triaxial cell are necessary for carrying out the UE1 and UE2 tests. The loading cap is provided with a threaded hole at the center, while the loading ram is provided with a bayonet catch at the top and threads at the bottom. The bored threaded hole in the loading cap was used as a guide during the consolidation process. When the extension test is to be started, the ram is screwed into the loading cap and pushed through a slotted plate mounted onto the proving ring, and engaged by rotating the ram through 90 degrees.

All the tests were carried out beyond the point of failure. The mode of failure was noted in all the tests. Water contents were measured after completion of the tests.

4. Hollow Cylinder Triaxial Tests

UI1, UI2 and UI3 tests were carried out in the hollow cylinder triaxial cell with controlled stress increments. The cell was placed on a balance scale provided with an adjustable yoke, controlled by a hand wheel. Dead loads were applied to the sample by balancing the yoke against the loading ram. Axial dead loads of 2.5 and 5.0 kilograms were applied to the specimens normally-consolidated under all-around pressures of 3 and 4 kg./cm.^{2} respectively. A period of 10 minutes was allowed for equilibrium to be attained for each increment. The pressure difference between the bore and the outside chambers, measured by a mercury manometer, was applied at the rate of 0.05 kg./cm.^{2} every 10 minutes.

In the UI2 tests, the bore chamber pressure was maintained constant by a Norwegian constant pressure cell while the outside chamber pressure was increased by a lever-screw until the desired amount of pressure difference was reached. The outside chamber pressure was then maintained constant by a Norwegian constant pressure cell throughout the test. The specimen was then axially-loaded by increments to failure.

In the UI1 tests, the specimen was first axially-loaded by increments, followed by increasing the outside chamber pressure until failure has been reached, while maintaining both the axial load and the bore chamber pressure constant.

In the UI3 tests, the axial stress was applied first and kept constant by taking weights off the scale when the outside chamber pressure was increased by the following

$$\text{axial dead load decrease} = (p_o - p_i)\,\frac{\pi}{4}\,(4)^2\,(2.54)^2$$

$$= 81\,(p_o - p_i)$$

The bore chamber pressure was kept constant throughout the test.

The tests were stopped as soon as failure was reached. The mode of failure was noted in all the tests. Water contents were measured after completion of the tests.

A2. DATA

Table 11A

Test: UC1 $\sigma_c = 3\text{kg./cm.}^2 \begin{cases} w_i = 42.5\% \\ w_f = 29.3\% \end{cases}$

ϵ_z %	$\bar{\sigma}_1$	$\bar{\sigma}_2$	$\bar{\sigma}_3$	$D=(\bar{\sigma}_1-\bar{\sigma}_3)$	$(\bar{\sigma}_1+\bar{\sigma}_3)/2$	Δu
0.000	2.87	2.87	2.87	0.00	2.87	0.00
0.185	3.33	2.74	2.74	0.59	3.04	0.13
0.304	3.46	2.70	2.70	0.76	3.08	0.17
0.490	3.84	2.49	2.49	1.35	3.17	0.38
0.85	3.93	2.16	2.16	1.77	3.05	0.71
1.00	3.90	2.05	2.05	1.85	2.98	0.82
1.46	3.89	1.89	1.89	2.00	2.89	0.98
2.28	3.80	1.65	1.65	2.15	2.73	1.22
3.02	3.72	1.50	1.50	2.22	2.61	1.37
4.05	3.63	1.35	1.35	2.28	2.49	1.52
5.24	3.58	1.25	1.25	2.33	2.42	1.62
6.55	3.53	1.15	1.15	2.38	2.34	1.72
7.90	3.47	1.05	1.05	2.42	2.26	1.82
9.55	3.51	1.05	1.05	2.46	2.28	1.82
10.75	3.52	1.03	1.03	2.49	2.28	1.84
13.30	3.53	1.03	1.03	2.50	2.28	1.84

Table 11B

Test: UC1 $\sigma_c = 4$ kg./cm.^{2} $\begin{cases} w_i = 41\% \\ w_f = 28.2\% \end{cases}$

ϵ_z %	$\bar{\sigma}_1$	$\bar{\sigma}_2$	$\bar{\sigma}_3$	$D=(\bar{\sigma}_1-\bar{\sigma}_3)$	$(\bar{\sigma}_1+\bar{\sigma}_3)/2$	Δu
0.00	3.96	3.96	3.96	0.00	3.96	0.00
0.50	4.79	3.55	3.55	1.24	4.17	0.41
0.86	5.28	3.06	3.06	2.22	4.17	0.90
1.13	5.14	2.68	2.68	2.46	3.91	1.28
1.54	5.08	2.38	2.38	2.70	3.73	1.58
2.00	5.05	2.20	2.20	2.85	3.63	1.76
2.85	4.96	1.98	1.98	2.98	3.47	1.98
3.95	4.78	1.76	1.76	3.02	3.27	2.20
5.07	4.65	1.57	1.57	3.08	3.11	2.39
6.30	4.58	1.46	1.46	3.12	3.02	2.50
7.45	4.53	1.38	1.38	3.15	2.96	2.58
8.70	4.54	1.36	1.36	3.18	2.95	2.60
10.42	4.51	1.31	1.31	3.20	2.91	2.65
13.40	4.54	1.31	1.31	3.23	2.93	2.65

Table 12

Test: UC2 $\sigma_c = 3$ kg./cm.^{2} $\begin{cases} w_i = 41.5\% \\ w_f = 27.6\% \end{cases}$

ϵ_z %	$\bar{\sigma}_1$	$\bar{\sigma}_2$	$\bar{\sigma}_3$	$D=(\bar{\sigma}_1-\bar{\sigma}_3)$	$(\bar{\sigma}_1+\bar{\sigma}_3)/2$	Δu
0.00	2.57	2.57	2.57	0.00	2.57	0.00
0.109	2.94	2.43	2.43	0.51	2.69	0.09
0.292	2.94	1.93	1.93	1.05	2.44	-0.01
0.802	3.12	1.72	1.72	1.40	2.42	-0.23
1.385	3.17	1.59	1.59	1.58	2.38	-0.30
1.82	3.15	1.55	1.55	1.60	2.35	-0.30
2.55	3.13	1.43	1.43	1.70	2.28	-0.30
3.28	3.11	1.35	1.35	1.76	2.23	-0.30
4.00	3.11	1.31	1.31	1.80	2.21	-0.31
5.10	3.09	1.22	1.22	1.87	2.16	-0.35
6.20	3.14	1.21	1.21	1.95	2.18	-0.42
7.30	3.18	1.11	1.11	2.07	2.15	-0.54
8.39	3.27	1.09	1.09	2.18	2.18	-0.64
9.12	3.29	1.11	1.11	2.18	2.20	-0.69
10.20	3.33	1.14	1.14	2.19	2.24	-0.77
12.40	3.36	1.11	1.11	2.25	2.24	-0.86
13.10	3.34	1.08	1.08	2.26	2.21	-0.89
13.85	3.38	1.10	1.10	2.28	2.25	-0.95
14.60	3.37	1.08	1.08	2.30	2.23	-0.98

Table 13A

Test: UI1 $\sigma_1 = 3$ kg./cm.^{2} $\begin{cases} w_i = 41.05\% \\ w_f = 29.53\% \end{cases}$

ϵ_z %	$\bar{\sigma}_1$	$\bar{\sigma}_2$	$\bar{\sigma}_3$	D= $(\bar{\sigma}_{max} - \bar{\sigma}_{min})$	$\frac{(\bar{\sigma}_{max} + \bar{\sigma}_{min})}{2}$	Δu
0.00	2.73	2.73	2.73	0.00	2.73	0.00
0.109	3.31	2.78	2.34	0.97	2.83	0.43
0.217	3.47	3.39	2.06	1.41	2.77	0.81
0.391	3.42	3.57	1.80	1.77	2.69	1.12
1.39	3.17	3.46	1.30	2.16	2.39	1.62
1.825	2.96	3.27	1.10	2.17	2.19	1.82
2.06	2.91	3.26	1.05	2.21	2.16	1.87
2.24	2.85	3.21	1.00	2.21	2.11	1.92
2.41	2.83	3.19	0.98	2.21	2.09	1.94
2.5+	2.98	3.71	1.05	2.66	2.38	1.97

Table 13B

Test: UI1 $\sigma_c = 4$ kg./cm.^{2} $\begin{cases} w_i = 45.50\% \\ w_f = 28.6\% \end{cases}$

ϵ_z %	$\bar{\sigma}_1$	$\bar{\sigma}_2$	$\bar{\sigma}_3$	D = $(\bar{\sigma}_{max} - \bar{\sigma}_{min})$	$\frac{(\bar{\sigma}_{max} + \bar{\sigma}_{min})}{2}$	Δu
0.00	3.83	3.83	3.83	0.00	3.83	0.00
0.202	3.99	3.81	3.81	0.18	3.90	0.02
0.302	4.45	3.74	3.74	0.71	4.10	0.09
0.470	4.97	3.56	3.56	1.41	4.27	0.27
0.582	5.33	4.63	3.25	2.12	4.29	0.76
0.761	5.32	5.09	2.74	2.58	4.03	1.34
0.940	5.30	5.31	2.49	2.82	3.90	1.64
1.12	5.24	5.38	2.33	3.05	3.79	1.83
1.50	5.08	5.36	2.07	3.29	3.58	2.11
2.02	5.01	5.42	1.90	3.52	3.46	2.31
2.91	4.99	5.54	1.79	3.75	3.39	2.44

Table 14A

Test: UI2 $\sigma_c = 3$ kg./cm.^{2} $\begin{cases} w_i = 41.4\% \\ w_f = 29.5\% \end{cases}$

ϵ_z %	$\bar{\sigma}_1$	$\bar{\sigma}_2$	$\bar{\sigma}_3$	D = $(\bar{\sigma}_{max} - \bar{\sigma}_{min})$	$\frac{(\bar{\sigma}_{max} + \bar{\sigma}_{min})}{2}$	Δu
0.00	2.63	2.63	2.63	0.00	2.63	0.00
0.00	2.67	2.78	2.57	0.21	2.68	0.09
0.096	2.83	3.30	2.31	0.99	2.81	0.45
0.214	3.15	3.21	2.22	0.99	2.72	0.54
0.30	3.40	3.14	2.15	1.25	2.78	0.61
0.45	3.70	2.96	1.97	1.73	2.84	0.79
0.60	3.78	2.80	1.81	1.97	2.80	0.95
0.90	3.83	2.64	1.65	2.18	2.74	1.11
1.30	3.89	2.53	1.54	2.35	2.72	1.22
1.67	3.85	2.43	1.44	2.41	2.65	1.32
2.78	3.76	2.28	1.29	2.47	2.53	1.47
4.70	3.58	2.08	1.09	2.49	2.34	1.67
7.05	3.49	1.98	0.99	2.50	2.24	1.77

Table 14B

Test: UI2 $\sigma_c = 4$ kg. /cm.^{2} $\begin{cases} w_i = 42.5\% \\ w_f = 28.7\% \end{cases}$

ϵ_z %	$\bar{\sigma}_1$	$\bar{\sigma}_2$	$\bar{\sigma}_3$	D = $(\bar{\sigma}_{max} - \bar{\sigma}_{min})$	$\frac{(\bar{\sigma}_{max} + \bar{\sigma}_{min})}{2}$	Δu
0.00	3.86	3.86	3.86	0.00	3.86	0.00
0.077	3.88	4.48	3.32	1.16	3.90	0.67
0.273	4.01	4.45	3.29	1.16	3.87	0.70
0.48	4.43	4.20	3.04	1.39	3.74	0.95
0.70	4.80	3.90	2.74	2.06	3.77	1.25
0.985	4.88	3.65	2.49	2.39	3.69	1.50
1.16	4.90	3.51	2.35	2.55	3.63	1.64
1.59	4.84	3.30	2.14	2.70	3.49	1.85
2.71	4.62	2.95	1.79	2.83	3.22	2.20
4.15	4.51	2.72	1.56	2.95	3.04	2.43
6.70	4.43	2.57	1.41	3.02	2.92	2.58
7.00	4.55	2.54	1.36	3.19	2.96	2.61

Table 15A

Test: UI3 $\sigma_c = 3$ kg./cm.^{2} $\begin{cases} w_i = 46\% \\ w_f = 30\% \end{cases}$

ϵ_z %	$\bar{\sigma}_1$	$\bar{\sigma}_2$	$\bar{\sigma}_3$	D = $(\bar{\sigma}_{max} - \bar{\sigma}_{min})$	$\frac{(\bar{\sigma}_{max} + \bar{\sigma}_{min})}{2}$	Δu
0.00	2.86	2.86	2.86	0.00	2.86	0.00
0.41	3.00	2.83	2.83	0.17	2.92	0.03
0.481	3.28	2.78	2.78	0.50	3.03	0.08
0.542	3.41	2.75	2.75	0.66	3.08	0.11
0.650	3.65	2.66	2.66	0.99	3.16	0.20
0.866	3.87	2.55	2.55	1.32	3.21	0.31
0.910	3.79	2.55	2.33	1.46	3.06	0.56
1.00	3.26	3.50	1.95	1.55	2.73	1.09
1.06	2.91	3.89	1.67	2.22	2.78	1.44
1.08	2.76	3.99	1.58	2.41	2.79	1.59
1.28	2.51	4.48	1.37	3.11	2.93	1.84

Table 15B

Test: UI3 $\sigma_c = 4$ kg./cm.^{2} $\begin{cases} w_i = 42.8\% \\ w_f = 28.1\% \end{cases}$

ϵ_z %	$\bar{\sigma}_1$	$\bar{\sigma}_2$	$\bar{\sigma}_3$	D = $(\bar{\sigma}_{max} - \bar{\sigma}_{min})$	$\frac{(\bar{\sigma}_{max} + \bar{\sigma}_{min})}{2}$	Δu
0.00	3.65	3.65	3.65	0.00	3.65	0.00
0.044	3.96	3.62	3.62	0.34	3.79	0.03
0.088	4.11	3.60	3.60	0.51	3.86	0.05
0.132	4.26	3.58	3.58	0.68	3.92	0.07
0.198	4.41	3.55	3.55	0.86	3.98	0.10
0.220	4.54	3.52	3.52	1.02	4.03	0.13
0.308	4.79	3.43	3.43	1.36	4.11	0.22
0.396	4.99	3.29	3.29	1.70	4.14	0.36
0.460	5.09	3.22	3.22	1.87	4.16	0.43
0.527	5.17	3.13	3.13	2.04	4.15	0.52
0.615	5.27	3.06	3.06	2.21	4.17	0.59
0.79	5.18	2.80	2.80	2.38	3.99	0.85
0.855	4.84	3.24	2.54	2.45	3.69	1.19
0.91	4.14	4.62	2.04	2.58	3.33	1.89
0.945	4.04	4.78	1.96	2.82	3.37	1.99
1.05	3.92	4.92	1.87	3.05	3.40	2.11
1.14	3.82	5.08	1.79	3.29	3.44	2.21
1.25	3.74	5.26	1.74	3.52	3.50	2.29
1.30	3.69	5.46	1.71	3.75	3.59	2.34
1.71	3.64	5.41	1.66	3.75	3.54	2.39

Table 16A

Test: UE1 $\sigma_c = 3$ kg./cm.^{2} $\begin{cases} w_i = 41.8\% \\ w_f = 27.02\% \end{cases}$

ϵ_z %	$\bar{\sigma}_1$	$\bar{\sigma}_2$	$\bar{\sigma}_3$	$D=(\bar{\sigma}_3-\bar{\sigma}_1)$	$(\bar{\sigma}_1+\bar{\sigma}_3)/2$	Δu
0.00	2.85	2.85	2.85	0.00	2.85	0.00
0.218	2.15	3.03	3.03	0.88	2.59	-0.18
0.436	1.96	2.98	2.98	1.02	2.47	-0.13
0.655	1.82	2.88	2.88	1.06	2.35	-0.03
0.874	1.70	2.80	2.80	1.10	2.25	+0.05
1.31	1.54	2.68	2.68	1.14	2.11	+0.17
2.18	1.37	2.58	2.58	1.21	1.98	+0.27
3.06	1.20	2.48	2.48	1.28	1.84	+0.37
3.93	1.12	2.46	2.46	1.34	1.79	+0.39
4.36	1.05	2.43	2.43	1.38	1.74	+0.42
5.24	0.90	2.39	2.39	1.49	1.65	+0.46
6.10	0.88	2.42	2.42	1.54	1.65	+0.43
7.42	0.79	2.48	2.48	1.69	1.64	+0.37
8.30	0.74	2.48	2.48	1.74	1.61	+0.37
9.17	0.72	2.48	2.48	1.76	1.60	+0.37
10.05	0.74	2.53	2.53	1.79	1.64	+0.32
10.90	0.75	2.58	2.58	1.83	1.67	+0.27
11.80	0.78	2.58	2.58	1.80	1.68	+0.27
12.67	0.79	2.59	2.59	1.80	1.69	+0.26
14.40	0.86	2.60	2.60	1.74	1.73	+0.25

Table 16B

Test: UE1 $\sigma_c = 4$ kg./cm.^{2} $\begin{cases} w_i = 42\% \\ w_f = 26.1\% \end{cases}$

ϵ_z %	$\bar{\sigma}_1$	$\bar{\sigma}_2$	$\bar{\sigma}_3$	$D = (\bar{\sigma}_3 - \bar{\sigma}_1)$	$(\bar{\sigma}_1 + \bar{\sigma}_3)/2$	Δu
0.00	3.81	3.81	3.81	0.00	3.81	0.00
0.218	2.86	4.05	4.05	1.19	3.46	-0.24
0.435	2.61	3.98	3.98	1.37	3.30	-0.17
0.870	2.31	3.81	3.81	1.50	3.06	0.00
1.31	2.10	3.68	3.68	1.58	2.89	+0.13
2.39	1.80	3.50	3.50	1.70	2.65	+0.31
3.48	1.61	3.43	3.43	1.82	2.52	+0.38
4.00	1.55	3.42	3.42	1.87	2.49	+0.39
5.22	1.34	3.40	3.40	2.06	2.37	+0.41
6.30	1.19	3.43	3.43	2.24	2.31	+0.38
7.82	1.08	3.48	3.48	2.40	2.28	+0.33
8.80	1.07	3.52	3.52	2.45	2.30	+0.29
10.43	1.07	3.60	3.60	2.53	2.34	+0.21
11.30	1.06	3.62	3.62	2.56	2.34	+0.19
12.20	1.08	3.62	3.62	2.54	2.35	+0.19
13.05	1.14	3.62	3.62	2.48	2.38	+0.19
14.80	1.26	3.62	3.62	2.36	2.42	+0.19

Table 17

Test: UE2 $\sigma_c = 4$ kg./cm.^{2} $\begin{cases} w_i = 42.1\% \\ w_f = 26.1\% \end{cases}$

ϵ_z %	$\bar{\sigma}_1$	$\bar{\sigma}_2$	$\bar{\sigma}_3$	$D=(\bar{\sigma}_3-\bar{\sigma}_1)$	$(\bar{\sigma}_1+\bar{\sigma}_3)/2$	Δu
0.00	3.84	3.84	3.84	0.00	3.84	0.00
0.19	4.43	5.24	5.24	0.81	4.84	0.40
0.58	3.94	5.36	5.36	1.39	4.67	0.93
1.16	3.35	4.91	4.91	1.56	4.13	1.58
1.55	2.98	4.58	4.58	1.60	3.78	1.91
2.71	2.39	4.09	4.09	1.70	3.24	2.50
4.25	1.84	3.69	3.69	1.85	2.77	3.00
5.81	1.68	3.66	3.66	1.98	2.67	3.08
6.65	1.62	3.66	3.66	2.04	2.64	3.08
6.98	1.70	3.76	3.76	2.06	2.73	3.08
7.35	1.72	3.76	3.76	2.04	2.74	3.08
8.15	1.68	3.61	3.61	1.93	2.65	3.13
9.70	1.73	3.66	3.66	1.93	2.70	3.08
12.00	1.79	3.53	3.53	1.74	2.66	3.01
13.60	1.80	3.38	3.38	1.58	2.59	3.01

A3. SAMPLE CALCULATIONS

1. <u>UC1 Test</u>: $\sigma_c = 3$ kg./cm.^{2}

Before consolidation:

Length of sample = 5''

Area of sample = 35. 4 sq. cm.

Volume of sample = 450 c. c.

After consolidation:

Volume of sample = 341. 8 c. c.

Length of sample = $5 \sqrt[3]{341.8/450} = 4.6''$

Area of sample = $(341.8/450)^{2/3} \times 35.4 = 29.5$ sq. cm.

Axial compression = 0. 046'' $\epsilon_z \% = \dfrac{0.046}{4.6} \times 100 = 1.0\%$

Axial load = 55 kg.

Cell pressure $\sigma_3 = 4$ kg./cm.^{2}

Pore-pressure u = 1. 95 kg./cm.^{2}

Deviator stress $D = \sigma_1 - \sigma_3 = \dfrac{55\ (4.6-0.046)}{29.5 \times 4.6}$

$= 1.85$ kg./cm.^{2}

$\sigma_1 = \sigma_3 + D = 4.0 + 1.85 = 5.85$ kg./cm.^{2}

$\bar{\sigma}_1 = \sigma_1 - u = 5.85 - 1.95 = 3.90$ kg./cm.^{2}

$\bar{\sigma}_3 = \sigma_3 - u = 4.00 - 1.95 = 2.05$ kg./cm.^{2}

2. <u>UC2 Test</u>: $\sigma_c = 3$ kg./cm.^{2}

Before consolidation

$L = 3''$ $\quad A = 10$ cm.^{2} $\quad V = 76$ c.c.

After consolidation

$L = 2.75''$ $\quad A = 8.44$ sq. cm. $\quad V = 58$ c.c.

Axial compression = 0.11'' $\quad \epsilon_z\% = \dfrac{0.11}{2.75} \times 100 = 4.0\%$

Load dial $\delta = 95$ div.

Cell pressure $\sigma_3 = 2.43$ kg./cm.^{2}

Pore-pressure $u = 1.12$ kg./cm.^{2}

Proving ring factor $N = 0.33$ lb./div.

$$\text{Deviator stress } D = \sigma_1 - \sigma_3 = 95 \times 0.33 \times 0.4545 \frac{(2.75 - 0.11)}{2.75 \times 8.44}$$

$$= 1.8 \text{ kg./cm.}^2$$

$\sigma_1 = \sigma_3 + D = 2.43 + 1.8 = 4.23$ kg./cm.^{2}

$\bar{\sigma}_1 = \sigma_1 - u = 4.23 - 1.12 = 3.11$ kg./cm.^{2}

$\bar{\sigma}_3 = \sigma_3 - u = 2.43 - 1.12 = 1.31$ kg./cm.^{2}

$\bar{\sigma}_2 = \bar{\sigma}_3 = 1.31$ kg./cm.^{2}

3. <u>UII Test:</u> $\sigma_c = 3$ kg./cm.^{2}

Before consolidation

$L = 5''$ $\quad$ $A = 35.4$ sq. cm. $\quad$ $V = 450$ c.c.

After consolidation

$L = 4.6''$ $\quad$ $A = 30$ sq. cm. $\quad$ $V = 350$ c.c.

$R_o = 2''$ $\quad$ $R_i = 1.585''$ $\quad$ $K = R_o/R_i = 1.26$

Axial compression = 0.018'' $\quad$ $\epsilon_z = \frac{0.018}{4.6} \times 100 = 0.391\%$

Axial load = 22.5 kg.

Outside chamber $p_o = 4.4$ kg./cm.^{2}

Bore chamber $p_i = 4.0$ kg./cm.^{2}

Pore-pressure $u = 2.4$ kg./cm.^{2}

$\Delta\sigma_1$ due to axial load $= \frac{22.5\,(4.6 - 0.018)}{30 \times 4.6}$

$\Delta\sigma_1$ due to $(p_o - p_i) = \frac{\pi}{4}(4 \times 2.54)^2\,(4.4 - 4.0)\,\frac{(4.6 - 0.018)}{20 \times 4.6}$

Total $\Delta\sigma_1$ due to axial load and $(p_o - p_i)$

$$= \left(\frac{4.6 - 0.018}{30 \times 4.6}\right)\left[22.5 + \frac{\pi}{4}(4 \times 2.54)^2\,(4.4 - 4.0)\right]$$

$$= 1.82 \text{ kg./cm.}^2$$

$\sigma_1 = p_i + \Delta\sigma_1 = 4.0 + 1.82 = 5.82$ kg./cm.^{2}

$\bar{\sigma}_1 = \sigma_1 - u = 5.82 - 2.40 = 3.42$ kg./cm.^{2}

Equation (25)

$$\sigma_2 = [4 + \frac{3 \times 1.26^2 + 1}{2\,(1.26^2 - 1)}\,(4.4 - 4.0)\,] = 5.97 \text{ kg./cm.}^2$$

$$\sigma_3 = (\frac{4.0 + 4.4}{2}) = 4.20 \text{ kg./cm.}^2$$

$$\bar{\sigma}_2 = \sigma_2 - u = 5.97 - 2.40 = 3.57 \text{ kg./cm.}^2$$

$$\bar{\sigma}_3 = \sigma_3 - u = 4.20 - 2.40 = 1.80 \text{ kg./cm.}^2$$

$$D = \sigma_2 - \sigma_3 = 3.57 - 1.80 = 1.77 \text{ kg./cm.}^2$$

4. <u>UI2 Test:</u> $\sigma_c = 3$ kg./cm.^{2}

Before consolidation

L = 5'' A = 35.4 sq. cm. V = 450 c.c.

After consolidation

L = 4.68'' A = 31 sq. cm. V = 358.8 c.c.

R_o = 2'' R_i = 1.57'' $K = R_o/R_i = 1.272$

Axial compression = 0.061'' $\epsilon_z = 1.3\%$

Axial load = 57.5 kg.

Outside chamber p_o = 4.25 kg./cm.^{2}

Bore chamber p_i = 4.0 kg./cm.^{2}

Pore-pressure u = 2.59 kg./cm.^{2}

$$\Delta\sigma_1 \text{ due to axial load} = \frac{57.5\,(4.68 - 0.061)}{4.68 \times 31}$$

$$\Delta\sigma_1 \text{ due to } (p_o - p_i) = \frac{\pi}{4}\,(4 \times 2.54)^2\,(4.25 - 4.0)\,(\frac{4.68 - 0.061}{4.6 \times 31})$$

Total $\Delta\sigma_1$ due to axial load & $(p_o - p_i)$

$$= \left(\frac{4.68 - 0.061}{4.6 \times 31}\right)\left[57.5 + \frac{\pi}{4}(4 \times 2.54)^2(4.25 - 4.0)\right] = 2.48 \text{ kg./cm.}^2$$

$$\sigma_1 = p_i + \Delta\sigma_1 = 4.0 + 2.48 = 6.48 \text{ kg./cm.}^2$$

$$\bar{\sigma}_1 = \sigma_1 - u = 6.48 - 2.59 = 3.89 \text{ kg./cm.}^2$$

Equation (25):

$$\sigma_2 = \left[4 + \frac{3 \times 1.272^2 + 1}{2(1.272^2 - 1)}(4.25 - 4.0)\right] = 5.12 \text{ kg./cm.}^2$$

$$\sigma_3 = \left(\frac{4.0 + 4.25}{2}\right) = 4.13 \text{ kg./cm.}^2$$

$$\bar{\sigma}_2 = \sigma_2 - u = 5.12 - 2.59 = 2.53 \text{ kg./cm.}^2$$

$$\bar{\sigma}_3 = \sigma_3 - u = 4.13 - 2.59 = 1.54 \text{ kg./cm.}^2$$

$$D = \sigma_1 - \sigma_3 = 3.89 - 1.54 = 2.35 \text{ kg./cm.}^2$$

5. <u>UI3 Test</u>: $\sigma_c = 3$ kg./cm.^{2}

Before consolidation

$L = 5''$ $\quad$ $A = 35.4$ sq. cm. $\quad$ $V = 450$ c.c.

After consolidation

$L = 4.61''$ $\quad$ $A = 30$ sq. cm. $\quad$ $V = 352$ c.c.

$R_o = 2''$ $\quad$ $R_i = 1.59''$ $\quad$ $K = R_o/R_i = 1.26$

Axial compression = 0.046'' $\quad$ $\epsilon_z = 1.0\%$

Axial load = 45 kg.

Outside chamber $p_o = 4.35$ kg./cm.^{2}

Bore chamber p_i = 4.0 kg./cm.^{2}

Pore-pressure u 2.23 kg./cm.^{2}

$\Delta\sigma_1$ due to axial load $= \dfrac{45\,(4.61 - 0.046)}{30 \times 4.61} = 1.49$ kg./cm.^{2}

$\Delta\sigma_1$ remains constant throughout the test.

$\sigma_1 = p_i + \Delta\sigma_1 = 4.0 + 1.49 = 5.49$ kg./cm.^{2}

$\bar{\sigma}_1 = \sigma_1 - u = 5.49 - 2.23 = 3.26$ kg./cm.^{2}

Equation (25):

$$\sigma_2 = [4 + \frac{3 \times 1.26^2 + 1}{2\,(1.26^2 - 1)}\,(4.35 - 4.0)] = 5.73 \text{ kg./cm.}^2$$

$$\sigma_3 = (\frac{4 + 4.35}{2}) = 4.18 \text{ kg./cm.}^2$$

$$\bar{\sigma}_2 = \sigma_2 - u = 5.73 - 2.23 = 3.50 \text{ kg./cm.}^2$$

$$\bar{\sigma}_3 = \sigma_3 - u = 4.18 - 2.23 = 1.95 \text{ kg./cm.}^2$$

$$D = \sigma_2 - \sigma_3 = 3.50 - 1.95 = 1.55 \text{ kg./cm.}^2$$

6. <u>UE1 Test</u>: σ_c = 3 kg./cm.^{2}

Before consolidation

L = 2.5'' A = 10 sq. cm. V = 63.5 c.c.

After consolidation

L = 2.29'' A = 8.37'' V = 48.6 c.c.

Axial extension = 0.07'' ϵ_z = 3.06%

Load dial δ = 69 div.

Cell pressure σ_3 = 4.5 kg./cm.^{2}

Pore-pressure u = 2.02 kg./cm.^{2}

Proving ring factor N = 0.33 lb./div.

Deviator stress $D = \sigma_3 - \sigma_1 = 69 \times 0.33 \times 0.4545 \frac{(2.29 - 0.07)}{2.29 \times 8.37}$

$= 1.28$ kg./cm.^{2}

$\sigma_1 = \sigma_3 - D = 4.5 - 1.28 = 3.22$ kg./cm.^{2}

$\bar{\sigma}_1 = \sigma_1 - u = 3.22 - 2.02 = 1.2$ kg./cm.^{2}

$\bar{\sigma}_2 = \bar{\sigma}_3 = \sigma_3 - u = 4.5 - 2.02 = 2.48$ kg./cm.^{2}

7. UE2 Test

Before consolidation

L = 2.8'' A = 10 sq. cm. V = 71.1 c.c.

After consolidation

L = 2.58'' A = 9.22 sq. cm. V = 60.3 c.c.

Axial compression = 0.11 ϵ_z = 4.25%

Load dial δ = 109 div.

Cell pressure σ_3 = 7.85 kg./cm.^{2}

Pore-pressure u = 4.16 kg./cm.^{2}

Proving ring factor N = 0.33 lb./div.

Deviator stress D $= \sigma_3 - \sigma_1 = 109 \times 0.33 \times 0.4545 \dfrac{(2.58 - 0.11)}{2.58 \times 9.22}$

$= 1.85$ kg./cm.^{2}

$\sigma_1 = \sigma_3 - D = 7.85 - 1.85 = 6.00$ kg./cm.^{2}

$\bar{\sigma}_1 = \sigma_1 - u = 6.00 - 4.16 = 1.84$ kg./cm.^{2}

$\bar{\sigma}_2 = \bar{\sigma}_3 = \sigma_3 - u = 7.85 - 4.16 = 3.69$ kg./cm.^{2}